Naval Surface Warfare Center
Carderock Division
West Bethesda, MD 20817-5700

NSWCCD-61-TM-2015/35 **December 2015**

Survivability, Structures, and Materials Department

Technical Report

Piezomagnetic Constant Variations in Galfenol Alloys Due to Sample Mounting and Alloy Preparation

by

J. B. Restorff, M. Wun-Fogle, Eric Summers

Naval Surface Warfare Center
Carderock Division
West Bethesda, MD 20817-5700

NSWCCD-61-TM-2015/35 **December 2015**

Survivability, Structures, and Materials Department
Technical Report

Piezomagnetic Constant Variations in Galfenol Alloys Due to Sample Mounting and Alloy Preparation

by

J. B. Restorff, M. Wun-Fogle, Eric Summers

REPORT DOCUMENTATION PAGE

Form Approved
OMB No. 0704-0188

1. REPORT DATE *(DD-MM-YYYY)*	2. REPORT TYPE	3. DATES COVERED *(From - To)*
December ??, 2015	Technical Report	9/2010 – 11/2015

4. TITLE AND SUBTITLE

Piezomagnetic Constant Variations in Galfenol Alloys Due to Sample Mounting and Alloy Preparation

5a. CONTRACT NUMBER N/A

5b. GRANT NUMBER N/A

5c. PROGRAM ELEMENT NUMBER 0602747N

6. AUTHOR(S)

James B. Restorff, Marilyn Wun-Fogle, and Eric Summers

5d. PROJECT NUMBER N/A

5e. TASK NUMBER

5f. WORK UNIT NUMBER

7. PERFORMING ORGANIZATION NAME(S) AND ADDRESS(ES) AND ADDRESS(ES)

Naval Surface Warfare Center
Carderock Division
9500 MacArthur Blvd.
West Bethesda, MD 20817-5700

ETREMA Products, Inc.
2500 North Loop Drive
Ames, IA 50010

8. PERFORMING ORGANIZATION REPORT NUMBER

NSWCCD-61-TR-2015/35

9. SPONSORING / MONITORING AGENCY NAME(S) AND ADDRESS(ES)

Office of Naval Research
Code 321MS
One Liberty Center
875 N. Randolph Street, Suite 1425
Arlington, VA 22203-1995

10. SPONSOR/MONITOR'S ACRONYM(S)

11. SPONSOR/MONITOR'S REPORT NUMBER(S) NA

12. DISTRIBUTION / AVAILABILITY STATEMENT

DISTRIBUTION STATEMENT A: Approved for public release; distribution is unlimited.

13. SUPPLEMENTARY NOTES

14. ABSTRACT:

This document reports on the results of the characterization of three varieties of Galfenol-18.4 ($Fe_{81.6}Ga_{18.4}$) and Galfenol-18.4 steel rods. Galfenol steel has a small portion of the iron replaced by low carbon steel. This adds small amounts of carbon as well as small amounts of the tramp elements contained in the steel. Rods were grown by free standing zone melt (FSZM) or an advanced Bridgman (AB) technique. Magnetic induction *B* and strain *S* were measured as a function of magnetic field *H* at constant stresses of –27.6, –55.2, and –82.7 MPa. The piezomagnetic constants d_{33} and μ_{33} varied in shape and size not only due to composition, but also among similar samples and different mountings of the same sample in the experimental appartus. Surprisingly, the largest variations due to mounting occurred in the samples with the highest d_{33}'s. Both the d_{33} and μ_{33} data were fit to Gaussians. Comparisons of data and model *S-H* curves are presented. The *B-H* hysteresis was 1100 ± 100 J/m^3 for all of the samples.

15. SUBJECT TERMS

Galfenol, piezomagnetic constant, permeability

16. SECURITY CLASSIFICATION OF: UNCLASSIFIED			17. LIMITATION OF ABSTRACT	18. NUMBER OF PAGES	19a. RESPONSIBLE PERSON
a. REPORT	b. ABSTRACT	c. THIS PAGE			19b. TELEPHONE NUMBER
UNCLASSIFIED	UNCLASSIFIED	UNCLASSIFIED	SAR		

CONTENTS

Page

FIGURES

Page

TABLES

Page

ADMINISTRATIVE INFORMATION

Performing organization: Magnetic Materials Group, Metallurgy and Fasteners Branch, (Code 612), Naval Surface Warfare Center, Carderock Division

Sponsor: Office of Naval Research, Code 321MS, Program element: 0602747N

Collaborator: Eric Summers, ETREMA Products, Inc.

ACKNOWLEDGEMENTS

This work was supported by the Office of Naval Research, Code 321 Maritime Sensing.

This page intentionally left blank

ABSTRACT

This document reports on the results of the characterization of the magnetic properties of three varieties of Galfenol-18.4 ($Fe_{81.6}Ga_{18.4}$) and Galfenol-18.4 steel rods. Galfenol steel has a small portion of the iron replaced by low carbon steel. This adds small amounts of carbon as well as small amounts of the tramp elements contained in the steel. Rods were grown by free standing zone melt (FSZM) or an advanced Bridgman (AB) technique. Magnetic induction B *and strain* S *were measured as a function of magnetic field* H *at constant stresses of –27.6, –55.2, and –82.7 MPa. The piezomagnetic constants* d_{33} *and* μ_{33} *varied in shape and size not only due to composition, but also among similar samples and different mountings of the same sample in the experimental apparatus. Surprisingly, the largest variations due to mounting occurred in the samples with the highest* d_{33}*'s. Both the* d_{33} *and* μ_{33} *data were fit to Gaussians. Comparisons of data and model* S-H *curves are presented. The* B-H *hysteresis was 1100 ± 100 J/m*^{3} *for all of the samples.*

INTRODUCTION

The iron-gallium alloy Galfenol is a relatively new magnetostrictive material with properties that are unique among active transducer materials. Galfenol has strains of approximately 400×10^{-6} in single crystal form [1] and an estimated linear portion of the strain of around $200 – 250 \times 10^{-6}$ in the easier-to-manufacturer highly textured polycrystal form.[2] Its most unique feature is the ability to withstand substantial amounts of tension, typically up to 350 MPa [2]; other active materials, e.g. Terfenol-D, PZT and the single crystal ferroelectrics are brittle and cannot withstand tension or torque. Another extraordinary property is the large operational temperature range. A single composition can be used between liquid helium and 150 $^{\circ}$C with little loss of magnetostriction. (The magnetostriction drops to one-half of its room temperature value at 300 $^{\circ}$C. [3]) Galfenol can be welded, machined, and forged with ordinary metal working tools. Finally, by annealing under stress it can provide nearly full magnetostriction at 40 MPa of tension [4]; annealing with a magnetic field applied offers full performance with no preload [5]. The $Fe_{81.6}Ga_{18.4}$ composition used in this paper is the most widely used composition.

The magnetostriction of Galfenol increases with gallium content more or less parabolically until the gallium content reaches ~19 percent.[1] Further gallium additions prompt

a phase change that severely reduces the magnetostriction. A second peak in magnetostriction appears with a gallium content of ~30 percent, but the modulus of the material is 7.9 GPa, about one-half of the value at $Fe_{81.6}Ga_{18.4}$. [6] The low modulus reduces the mechanical energy that can be obtained compared to the $Fe_{81.6}Ga_{18.4}$ composition and is also more expensive because of the higher gallium content.

This paper describes the piezomagnetic constant d_{33} and permeability μ_{33} as a function of magnetic field H under compressive stresses of –27.6, –55.2, and –82.7 MPa. Samples were removed from the test apparatus, remounted and remeasured multiple times. The area of the magnetic flux density B vs. H (B-H) loops was determined. The resulting d_{33}'s and μ_{33}'s were fit to Gaussians. The nomenclature used in this paper generally follows IEEE Std. 319-1990. S is the strain, T is the stress (compressive stresses are negative), s is the compliance, d is the piezomagnetic constant, and μ is the permeability. The magnetization M (A/m) is reported as the intrinsic magnetic flux density J (tesla), where $J = \mu_0 M$.

EXPERIMENT

Table I lists the samples used in this study. The samples were 6.35 mm diameter rods approximately 53 mm long. Two Micro-Measurements WK-06-500GB-350 strain gages were mounted on opposite sides of the samples using the Micro-Measurements AE-15 resin system. The measurements were conducted on an MTS 858 load frame with a custom sample holder used in constant stress mode. The sample holder included a drive coil, a pick-up coil to measure B, and a Hall probe located as close to the sample as practicable to measure H. A schematic of the sample holder is shown in Fig. 1. As H changes during the experiment, the permeability μ of the sample also changes, typically by a factor of ~3. The variation in μ affects the magnetic circuit which in turn changes H across the sample in a non-simple way. In order to correct for this, the magnetic field was actively controlled; see Ref. 7 for a discussion of this and a description of the H control system. The magnetic field was cycled and B-H and S-H curves were obtained.

The samples were characterized using a simple one-domain rotation described in Ref. 8 that has proven useful in the past for this purpose. The model calculates the energy E with the magnetization direction α at 2048 equally spaced directions.

$$E = -J_s H\alpha_z + K_{\text{cubic}}\left(\alpha_x^4 + \alpha_y^4 + \alpha_z^4\right) + \alpha_z^2\left(K_{\text{uniaxial}} - \lambda_{\text{sat}} T\right) \quad (1)$$

where J_s is the saturation magnetization, H is the applied magnetic field, T is the applied stress, and $\lambda_{\text{sat}} = (3/2)\ \lambda_{100}$ is the saturation magnetostriction. K_{cubic} is related to the conventional cubic anisotropy K_1 by $K_{\text{cubic}} = -K_1 / 2$. A uniaxial anisotropy K_{uniaxial} can be built into the sample by stress or field annealing [4, 5]. Small residual values of K_{uniaxial} also appear during sample growth. An energy weighted average (Eq. 2) is used to calculate the magnetization and strain. The smoothing factor Ω is intended to mimic the contribution of strain, composition, alignment, and stress inhomogeneities in the sample.

$$S = \frac{\sum_i S_i \exp(-E_i / \Omega)}{\sum_i \exp(-E_i / \Omega)} \text{ and } J = \frac{\sum_i M_i \exp(-E_i / \Omega)}{\sum_i \exp(-E_i / \Omega)} \quad (2)$$

where S and J are the model strain and magnetization, respectively, and $S_i = \lambda_{sat}\alpha_z^2$ and $J_i = J_s\alpha_z$ and i is an index over the α's. The uniaxial anisotropy term K_{uniaxial} describes an anisotropy parallel to the rod axis and mimics an applied stress $T = K_{\text{uniaxial}} / \lambda_{\text{sat}}$ both in the model and in real samples. The values shown in the Tables II, III, IV, V, VI, and VII are averages and standard deviations obtained from multiple mountings of the same sample. Note that the saturation magnetostriction S_{sat} and magnetization J_{sat} given in Table I have almost no error while the other parameters can vary substantially as a function of the sample mounting.

The saturation magnetostriction S_{sat} is moderately well correlated ($R = -0.77$) with the cubic anisotropy K_{cubic}; see Fig. 2. Presumably, a higher value of K_{cubic} implies a more single-crystal like texture of the grains.[9] The value of Ω is also moderately well correlated ($R = -0.81$) with the maximum d_{33} / S_{sat}; see Fig. 3. The parameter Ω describes the shape of $d_{33}(H)$ and K_{cubic} sets the amplitude.

RESULTS

While the d_{33} measurements were very repeatable during a single sample mount, it was found that the shape and amplitude of the d_{33} curves were dependent on the mounting of the sample in the apparatus which apparently varied slightly with each removal and remounting. Figure 4 shows repeated measurements on sample GsF1 during a single mount. Figure 5 shows the variation in d_{33} when the sample was removed and remounted between each measurement. The higher magnetostriction samples were more sensitive to the mounting and extreme care in mounting the samples produced more consistent results. Yoo, et al. examined laminations cut from rods similar to ones used in this study and found that a large fraction of the volume consisted of only 6 – 8 grains.[10] We postulate that slight changes in the alignment of the samples could result in a higher stress being applied to one grain or another. In the model, a misalignment of only 5 degrees was sufficient to produce a noticeable change in magnetostriction.

We also determined the hysteresis of the rods from the *B*-*H* loops. The fractional error is large, about ten percent, due mainly to the small size of the hysteresis, which is about one-tenth of the hysteresis of Terfenol-D [11], for example. The average of more than 350 hysteresis loops taken from all of the Fe-Ga samples except for the field annealed samples GsAh1 and GsAh2 was 1100 ± 100 J/m^3. The uncertainty in the measured hysteresis was large enough to overwhelm any hysteresis changes due to applied stress or sample composition. The two field annealed samples had a strikingly higher hysteresis, 1900 ± 300 J/m^3 (average of 91 loops), which was about twice the value of the other Fe-Ga samples.

Gaussian Fits to the Data

We can use this data to generate a prediction of the output of a transducer using this material. The usual realization of a transducer consists of a rod of the magnetostrictive material with a drive coil wound around it. A magnetic bias is applied to move the operating point into the active region of the magnetostrictive material. Models of transduction devices commonly use the linearized version of the piezomagnetic equations

$$\begin{aligned} \Delta S_{33} &= s_{33}\Delta T_3 + d_{33}\Delta H_3 \\ \Delta B_3 &= d_{33}\Delta T_3 + \mu_{33}\Delta H_3 \end{aligned} \tag{3}$$

where the stress, magnetic field and strain are all in the direction along the rod axis denoted by "3". In reality, the situation is considerably more complex. The "constants" d_{33}, s_{33} and μ_{33} are, in fact, functions of *H*, *S*, temperature and even the history of the sample. The change in s_{33} and μ_{33} is typically a factor of three in Galfenol materials [6], although it can be considerably larger at certain combinations of stress and field in materials with "jumps," which occur when the moment switches from one low energy direction of the magnetocrystalline anisotropy to another. The change in μ_{33} alters the magnetic circuit and changes the effective bias field on the active material. Differentiating the *S*-*H* and *B*-*H* measured data includes all of the above effects and should lead to more realistic predictions. Gaussian shapes were used and s_{33} data at constant stress were fit to a Gaussian

$$A\exp\left(\frac{\left(H - H_{\text{center}} \pm H_{\text{shift}}\right)^2}{2\sigma^2}\right), \tag{4}$$

where *H* is magnetic field, H_{center} is the center of the Gaussian, σ is the width, *A* is the amplitude, and H_{shift} is a constant that describes the hysteresis and is positive for increasing fields and negative for decreasing fields. Since the d_{33} distribution in the data seemed to fall off slightly slower than the Gaussian distribution we also tried a Lorentz distribution (also called a Cauchy distribution); see Eq. 5. In some cases, this provided a slightly better fit; in others it was slightly worse. The differences were small in either case; we chose to use the mathematically better behaved Gaussian distribution.

$$\frac{A}{\pi\sigma\left[1+\left(\frac{H - H_{\text{center}} \pm H_{\text{shift}}}{\sigma}\right)^2\right]} \tag{5}$$

The piezomagnetic constant d33

After subtracting the shift in *H* due to hysteresis, d_{33} is an odd function of *H*. Because of that, the data was fit to two Gaussians, one in the $H > 0$ half-plane and a second, inverted, Gaussian in the $H < 0$ half-plane. Both Gaussians have the same amplitude, width and shift. This is necessary because the tails of the two Gaussians can overlap. In the overlap region, the contributions of the two Gaussians subtract and give a shape near $H = 0$ that cannot be modeled by a single Gaussian, i.e. the d_{33} curve in the $H > 0$ half-plane cannot be modeled with a single

Gaussian in the $H > 0$ half-plane. In this paper when we speak of a "single" Gaussian, we mean the "Gaussian / inverted Gaussian" described above.

Most fits could be improved by adding a second Gaussian. Usually the second Gaussian was a broad, low "base" that the primary peak sat atop. However, in some cases, better fits could be obtained by placing a narrow Gaussian in the high H tail of the primary Gaussian. In a few cases, using three Gaussians would have obviously improved the fit. In situations like this it is easy to fall into the trap of continuing to add Gaussian curves until one obtains a very good fit, but loses all sense of the underlying physical process. Because of this, we used only a single Gaussian, reasoning that the "lost" d_{33} occurred mostly at high or low fields, well away from the peak d_{33}, a region where most practical devices would not operate anyway. Figure 6 shows an example of the increasing H and decreasing H fits to data taken for Sample GA5 at –55.2 MPa. Figure 7 shows measured d_{33} for increasing H and individual fits for the last four mounts of the same sample and stress. These four data sets include a poor mount (Fig. 7a), which is one of the least Gaussian-like measurements taken during this study, and three more typical data sets. Tables II, III and IV show the d_{33} results of the fitting procedure. The values in the tables are the average and standard deviation computed from all of the mounts. The graphs showing the d_{33} curves for each of the samples used in this study can be found in the appendices.

Because d_{33} is defined as the derivative of the S-H curve, integrating d_{33} over all H should give the saturation magnetostriction, S_{sat}. In practice, we found that the Gaussian fits only captured 85 to 95 percent of S_{sat}. The "lost" magnetostriction likely resides in the long tails in the d_{33} data that are not well represented by the Gaussian.

The permeability μ_{33}

In contrast to d_{33}, after subtracting the shift in H due to hysteresis, μ_{33} is an even function of H. Because of that, a similar technique was used to fit the μ_{33} data except that the Gaussian in the $H < 0$ half-plane was not inverted. Also in contrast to the d_{33} fits, this did not produce satisfactory fits. The fit peaks were wider than the data peaks and the fit μ_{33} went to 0 near $H = 0$ which did not mimic the data well. When an additional Gaussian centered at $H = 0$ was added to the fits, the fits improved substantially and this model was used for μ_{33} throughout this paper. Tables V, VI, and VII show the μ_{33} results of the fitting procedure. The graphs showing the μ_{33} curves for each sample in this study can be found in the appendices.

DISCUSSION

The value of a fitting procedure depends entirely on how well it reproduces reality. The fact that d_{33} is a derivative of the *S*-*H* curve emphasizes discrepancies between the measured and fit d_{33}. A better indication of how useful the Gaussian fit is might be to compare the integrated fit d_{33} with the measured strain. Practical devices generally utilize a permanent magnet bias to set the operating point to the d_{33} maximum and operation is limited to the quasi-linear region of the *S*-*H* curve. Operation outside of this region requires higher applied fields, i.e. higher currents and undesirable I^2R heating while producing little additional strain. Figure 8 shows the integrated d_{33} fit, which should correspond to the *S*-*H* curve, plotted on top of the measured *S*-*H* data. The fits are the same fits displayed in Fig. 7. The three boxes represent using strains from 10 to 90 percent, 20 to 80 percent and 30 to 70 percent of S_{sat} correspond to using various extents of the quasi-linear region. The curves for these three ranges are shown superimposed upon one another but are so similar that they are hard to separate visually. The constant of integration is set by matching the measured and integrated strain at the lower left corner of the box. With the exception of Fig. 8a, the integrated fits are very close to the measured data except at the highest *H*. The atypical d_{33} shown in Fig. 7a produces an integrated *S* that differs noticeably from the data near $H = 150$ Oe.

We conclude that a simple fit of d_{33} to a Gaussian and μ_{33} to two Gaussians provide a useful model for Galfenol transducer modeling, and, at this point in time at least, manufacturing variations are large enough to be important. Finally, the samples with the highest piezomagnetic *d*-constant require the most precise mounting techniques.

CONCLUSIONS

We have measured *B*-*H* and *S*-*H* loops at various stresses for several types of Galfenol active materials and have derived d_{33} and μ_{33} from this data. The values of d_{33} and μ_{33} were found to vary as the sample was removed and then remounted. The samples with the highest d_{33}, i.e. the best samples, were found to be the most sensitive, presumably because they consisted of only a few large grains. Detailed graphs of:

1. magnetostriction *S* and magnetization *B* as a function of magnetic field *H* under several compressive stresses,
2. piezomagnetic constants d_{33} and relative permeability μ_{33} as a function of magnetic field *H* under several compressive stresses,
3. strain *S* and magnetization *B* as a function of stress *T* for several magnetic fields,
4. piezomagnetic constant d_{33}* and modulus *E* as a function of stress *T* for several magnetic fields,
5. magnetostriction *S* and magnetization *B* as a function of magnetic field *H* under a constant stress of –55.2 MPa for repeated mountings in the experimental apparatus,
6. piezomagnetic constant d_{33} and relative permeability μ_{33} as a function of magnetic field *H* under a constant stress of –55.2 MPa for repeated mountings in the experimental apparatus

for Galfenol ($Fe_{81.6}Ga_{18.4}$) FSZM samples can be found in Appendix A, for Galfenol ($Fe_{81.6}Ga_{18.4}$) Advanced Bridgman samples in Appendix B, and for Galfenol Steel ($Fe_{81.6}Ga_{18.4}$ + C) FSZM samples in Appendix C.

REFERENCES

1. Clark, A. E.; K. B. Hathaway, M. Wun-Fogle, J. B. Restorff, T. A. Lograsso, V. M. Keppens, G. Petculescu, and R. A. Taylor, "Extraordinary Magnetoelasticity and Lattice Softening in bcc Fe-Ga Alloys," *Journal of Applied Physics*, Vol. 93, No. 10, Parts 2 & 3, 2003, pp. 8621 – 8623.
2. See table titled "Galfenol Physical Properties" on *www.Etrema.com/galfenol/*.
3. Clark, A. E.; M. Wun-Fogle, J. B. Restorff, K. W. Dennis, T. A. Lograsso, and R. W. McCallum, "Temperature Dependence of the Magnetic Anisotropy and Magnetostriction of $Fe_{100-x}Ga_x$ (x = 8.6, 16.6, 28.5)," *Journal of Applied Physics*, Vol. 97, 2005, p. 10M316; Magnetostriction measurements between ~300 K to 575 K were obtained via private communication from Dr. Jin-Hyeong Yoo.
4. Wun-Fogle, M.; J. B. Restorff, A. E. Clark, Erin Dreyer, and Eric Summers, "Stress Annealing of Fe-Ga Transduction Alloys for Operation Under Tension and Compression," *Journal of Applied Physics*, Vol. 97, 2005, p. 10M301.
5. Yoo, J. H.; S.-M. Na, J. B. Restorff, M. Wun-Fogle, and A. B. Flatau, "The Effect of Field Annealing on Highly Textured Polycrystalline Galfenol Strips," *IEEE Transactions on Magnetics*, Vol. 45, 2009, pp. 4145 – 4148.
6. Petculescu, G.; K. B. Hathaway, T. A. Lograsso, M. Wun-Fogle, and A. E. Clark, "Magnetic Field Dependence of Galfenol Elastic Properties," *Journal of Applied Physics*, Vol. 97, 2005, pp. 10M315-1 to 10M315-3.
7. Wun-Fogle, M.; J. B. Restorff, and A. E. Clark, "Soft and Hard Elastic Moduli of Galfenol Transduction Elements," *Journal of Applied Physics*, Vol. 105, 2009, p. 07A923.
8. Restorff, J. B.; M. Wun-Fogle, A. E. Clark, and K. B. Hathaway, "Induced Magnetic Anisotropy in Stress-Annealed Galfenol Alloys," *IEEE Transactions on Magnetics*, Vol. 42, 2006, pp. 3087-3089.
9. For sixteen $Fe_{81.6}Ga_{18.4}$ samples, S_{sat} = (220 ± 15) – (1.7 ± 0.6) K_{cubic}; R = –0.61 with S_{sat} in μS and K_{cubic} in MJ/m^3. d_{33}^{max} = (130 ± 70) – (30 ± 40) Ω; R = –0.18 with d_{33}^{max} in nm/A and Ω in kJ/m^3.
10. Yoo, J.-H.; S.-M. Na, J. B. Restorff, M. Wun-Fogle, and A. B. Flatau, "The Effect of Field Annealing on Highly Textured Polycrystalline Galfenol Strips," *IEEE Transactions on Magnetics*, Vol. 45, 2009, pp. 4145 - 4148.
11. Wun-Fogle, Marilyn; James B. Restorff, Arthur E. Clark and Jon Snodgrass, "Magnetomechanical Damping Capacity of $Tb_xDy_{1-x}Fe_{1.92}$ ($0.30 < x < 0.5$) Alloys," *IEEE Transactions on Magnetics*, Vol. 39, 2003, pp. 3408-3410.

Table I. Sample characteristics obtained by using Eqs. 1 and 2.

NSWC	Sample	Composition	Growth	Sets	S_{sat} (μS)	J_{sat} (T)	K_{cubic} (kJ/m^3)	$K_{uniaxial}$ (kJ/m^3)	Ω (kJ/m^3)
1271	GF1	$Fe_{81.6}Ga_{18.4}$	FSZM	7	292 ± 2	1.63 ± 0.00	–25 ± 3	–1.8 ± 0.6	1.6 ± 0.4
1402	GF2	$Fe_{81.6}Ga_{18.4}$	FSZM	6	258 ± 1	1.59 ± 0.00	–21 ± 3	0.7 ± 0.5	2.3 ± 0.3
1529	GA1	$Fe_{81.6}Ga_{18.4}$	AB	6	277 ± 1	1.60 ± 0.01	–27 ± 4	–1.5 ± 0.8	2.0 ± 0.3
1530	GA2	$Fe_{81.6}Ga_{18.4}$	AB	4	255 ± 1	1.56 ± 0.01	–19 ± 1	–0.9 ± 0.3	1.5 ± 0.2
1531	GA3	$Fe_{81.6}Ga_{18.4}$	AB	5	250 ± 1	1.56 ± 0.00	–16 ± 1	–0.6 ± 0.3	1.3 ± 0.1
1532	GA4	$Fe_{81.6}Ga_{18.4}$	AB	5	236 ± 2	1.59 ± 0.00	–10 ± 1	2.5 ± 0.5	1.0 ± 0.1
1533	GA5	$Fe_{81.6}Ga_{18.4}$	AB	8	289 ± 2	1.65 ± 0.01	–36 ± 7	–2.6 ± 0.6	1.9 ± 0.3
1403	GsF1	$Fe_{81.6}Ga_{18.4}$ + C	FSZM	4	219 ± 1	1.61 ± 0.00	–19 ± 0.7	–1.8 ± 0.5	2.5 ± 0.1
1404	GsF2	$Fe_{81.6}Ga_{18.4}$ + C	FSZM	5	223 ± 3	1.54 ± 0.01	–5.5 ± 3	–0.2 ± 0.6	1.7 ± 0.5

Note. The number of Sets is the number of different mountings of the same sample in the experimental apparatus used to obtain the average and standard deviation. The sample naming convention uses “G” and “Gs” at the beginning of the sample name to indicate Galfenol or Galfenol steel respectively; the “A” or “F” indicates Advanced Bridgman or Free Standing Zone Melt growth techniques; and the number is a sequence number.

Table II. Weighted fit values of the piezomagnetic constant d_{33} for measurements taken under a compressive stress of –27.6 MPa.

NSWC ID	Sample ID	Fit Peak d_{33} (nm / A)	Data Peak d_{33} (nm / A)	20 – 80% d_{33} (nm / A)	Fractional Amplitude	Avg Frac Amp	Center (kA/m)	Width (kA/m)	H_{shift} (kA/m)
1271	GF1	81 ± 35	88 ± 38	72 ± 36	0.97 ± 0.07	1.12	5.9 ± 0.2	1.6 ± 0.6	0.29 ± 0.04
1402	GF2	29 ± 2	31 ± 2	27 ± 2	0.90 ± 0.01	0.90	7.5 ± 0.1	3.3 ± 0.3	0.28 ± 0.01
1529	GA1	61 ± 8	63 ± 10	56 ± 9	0.90 ± 0.02	0.92	6.8 ± 0.2	1.8 ± 0.3	0.3 ± 0.01
1530	GA2	65 ± 13	66 ± 13	57 ± 9	0.86 ± 0.03	0.88	5.8 ± 0.1	1.4 ± 0.3	0.30 ± 0.01
1531	GA3	68 ± 9	69 ± 9	59 ± 8	0.87 ± 0.02	0.88	5.6 ± 0.2	1.3 ± 0.2	0.30 ± 0.01
1532	GA4	54 ± 4	58 ± 5	50 ± 5	0.89 ±0.03	0.90	7.3 ± 0.2	1.6 ± 0.2	0.30 ± 0.01
1533	GA5	67 ± 12	73 ± 14	61 ± 12	0.94 ± 0.03	0.97	5.5 ± 0.2	1.7 ± 0.3	0.31 ± 0.01
1403	GsF1	…	…	…	…		…	…	…
1404	GsF2	…	…	…	…		…	…	…

Note. The values are the average and standard deviation computed from data for all of the sample mounts. *Fit Peak* is the highest point on the fitted Gaussian; *Data Peak* is the highest point on the data curve (neglecting "spikes"); *20 – 80% d_{33}* is the average slope of the *S*-*H* curve between 20 and 80 percent of S_{sat} *Gaussian Amplitude* is the value of *A* in Eq. 4; *Fractional Amplitude* is the fraction of S_{sat} captured by the Gaussian fit (see text); *Center* and *Width* are H_{center} and σ of Eq. 4; and H_{shift} is the shift in H_{center} due to hysteresis, i.e. the up and down curves are 2 x H_{shift} apart. The magnetostriction in GsF1 and GsF2 did not reach saturation at –27.6 MPa but did at higher stresses.

Table III. Weighted fit values of the piezomagnetic constant d_{33} for measurements taken under a compressive stress of –55.2 MPa. See Table II for a description of the column headers.

NSWC ID	Sample ID	Fit Peak d_{33} (nm / A)	Data Peak d_{33} (nm / A)	20 – 80% d_{33} (nm / A)	Fractional Amplitude	Avg Frac Amp	Center (kA/m)	Width (kA/m)	H_{shift} (kA/m)
1271	GF1	61.5 ± 27	64 ± 25	54 ± 27	0.97 ± 0.05	1.13	11.3 ± 0.2	2.1 ± 0.8	0.27 ± 0.03
1402	GF2	27 ± 2	30 ± 2	26 ± 2	0.91 ± 0.02	0.92	12.9 ± 0.3	3.5 ± 0.4	0.28 ± 0.01
1529	GA1	45 ± 7	47 ± 7	41 ± 6	0.91 ± 0.02	0.93	12.3 ± 0.4	2.4 ± 0.4	0.30 ± 0.01
1530	GA2	51 ± 12	53 ± 12	47 ± 10	0.87 ± 0.04	0.91	10.8 ± 0.1	1.8 ± 0.4	0.31 ± 0.01
1531	GA3	55 ± 9	56 ± 10	49 ± 7	0.87 ± 0.03	0.89	10.6 ± 0.3	1.6 ± 0.3	5.3 ± 1.8
1532	GA4	40 ± 5	42 ± 8	36 ± 4	0.93 ± 0.05	0.94	12.5 ± 0.4	2.2 ± 0.3	0.31 ± 0.01
1533	GA5	54 ± 15	59 ± 16	49 ± 14	0.95 ± 0.03	1.01	10.6 ± 0.3	2.1 ± 0.5	0.31 ± 0.01
1403	GsF1	21 ± 2	22 ± 2	20 ± 2	0.91 ± 0.004	0.91	9.6 ± 0.2	3.8 ± 0.4	0.33 ± 0.01
1404	GsF2	13.9 ± 0.4	14.4 ± 0.5	12.9 ± 0.4	0.91 ± 0.05	0.892	10.8 ± 0.3	6.2 ± 0.3	0.32 ± 0.01

Table IV. Weighted fit values of the piezomagnetic constant d_{33} for measurements taken under a compressive stress of –82.7 MPa. See Table II for a description of the column headers.

NSWC ID	Sample ID	Fit Peak d_{33} (nm / A)	Data Peak d_{33} (nm / A)	20 – 80% d_{33} (nm / A)	Fractional Amplitude	Avg Frac Amp	Center (kA / m)	Width (kA / m)	H_{shift} (kA / m)
1271	GF1	51 ± 21	52 ± 20	45 ± 20	0.96 ± 0.04	1.09	17 ± 0.3	2.5 ± 0.9	0.26 ± 0.02
1402	GF2	25.4 ± 2.2	28 ± 2	23 ± 2	0.89 ± 0.2	0.90	18.2 ± 1.2	3.6 ± 0.4	0.27± 0.01
1529	GA1	37 ± 6	39 ± 5	33 ± 5	0.89 ± 0.02	0.91	18.4 ± 0.6	2.9 ± 0.5	0.30 ± 0.01
1530	GA2	41 ± 8	43 ± 9	37 ± 7	0.87 ± 0.04	0.90	16.3 ± 0.2	2.2 ± 0.5	0.30 ± 0.01
1531	GA3	46 ± 8	49 ± 8	42 ± 8	0.88 ± 0.03	0.90	16 ± 0.4	1.9 ± 0.4	0.30 ± 0.011
1532	GA4	31 ± 5	33 ± 8	27 ± 3	0.93 ± 0.06	0.95	18.1 ± 0.5	2.9 ± 0.5	0.31 ± 0.01
1533	GA5	46 ± 19	49 ± 20	40 ± 17	0.96 ± 0.04	1.06	16 ± 0.4	2.7 ± 0.8	0.31 ± 0.02
1403	GsF1	18 ± 2	19 ± 2	17 ± 2	0.92 ± 0.01	0.93	14 ± 0.4	4.4 ± 0.6	0.32 ± 0.01
1404	GsF2	12.3 ± 0.5	12.6 ± 0.5	11.5 ± 0.4	0.92 ± 0.00	0.92	15.9 ± 0.3	6.8 ± 0.3	0.32 ± 0.03

Table V. Weighted fit values of the permeability μ33 for measurements taken under a compressive stress of –27.6 MPa.

NSWC ID	Sample ID	Fit Peak μ_{33} (nm / A)	Data Peak μ_{33} (nm / A)	20 – 80% μ_{33} (nm / A)	Fractional Amplitude	Avg Frac Amp	Center (kA / m)	Width (kA / m)	H_{shift} (kA / m)
1271	GF1	323 ± 137	366 ± 143	298 ± 146	1.01 ± 0.02	1.18	5.9 ± 0.2	1.7 ± 0.7	0.16 ± 0.03
1402	GF2	122 ± 7	134 ± 7	112 ± 8	0.96 ± 0.004	1.02	7.1 ± 0.1	3.8 ± 0.3	0.20 ± 0.03
1529	GA1	204 ± 32	236 ± 34	211 ± 31	0.97 ± 0.01	0.98	6.7 ± 0.3	1.7 ± 0.3	0.15 ± 0.01
1530	GA2	247 ± 52	288 ± 56	184 ± 35	1.01 ± 0.002	1.03	5.7 ± 0.1	1.2 ± 0.3	0.15 ± 0.01
1531	GA3	267 ± 42	299 ± 46	258 ± 36	1.01 ± 0.003	1.02	5.5 ± 0.1	1.2 ± 0.2	0.14 ± 0.01
1532	GA4	221 ± 14	264 ± 13	226 ± 18	1.01 ± 0.002	1.01	7.3 ± 0.2	1.5 ± 0.1	0.15 ± 0.01
1533	GA5	247 ± 41	304 ± 53	247 ± 45	1.00 ± 0.007	1.06	5.5 ± 0.3	1.6 ± 0.4	0.16 ± 0.01
1403	GsF1	…..	…..	…..	…..	…..	…..	…..	…..
1404	GsF2	…..	…..	…..	…..	…..	…..	…..	…..

Note. The values are the average and standard deviation computed from data for all of the sample mounts. Fit Peak is the highest point on the fitted Gaussian; Data Peak is the highest point on the data curve (neglecting "spikes"); 20 – 80% μ33 is the average slope of the B-H curve between 20 and 80 percent of Bsat; Gaussian Amplitude is the value of A in Eq. 4; Fractional Amplitude is the fraction of Bsat captured by the Gaussian fit (see text); Center and Width are Hcenter and σ of Eq. 4; and Hshift is the shift in Hcenter due to hysteresis, i.e. the up and down curves are 2 x Hshift apart.

Table VI. Weighted fit values of the permeability μ33 for measurements taken under a compressive stress of –55.2 MPa. See Table V for a description of the column headers.

NSWC ID	Sample ID	Fit Peak μ_{33} (nm / A)	Data Peak μ_{33} (nm / A)	20 – 80% μ_{33} (nm / A)	Fractional Amplitude	Avg Frac Amp	Center (kA/m)	Width (kA/m)	H_{shift} (kA/m)
1271	GF1	228 ± 98	250 ± 100	206 ± 101	1.01 ± 0.01	1.16	11.2 ± 0.2	2.2 ± 0.9	0.14 ± 0.02
1402	GF2	85 ± 9	115 ± 9	100 ± 8	1.11 ± 0.24	1.02	13.1 ± 0.2	3.1 ± 0.4	0.11 ± 0.01
1529	GA1	141 ± 23	168 ± 18	144 ± 20	1.01 ± 0.01	1.02	12.1 ± 0.5	2.3 ± 0.4	0.15 ± 0.01
1530	GA2	182 ± 40	213 ± 45	184 ± 35	1.02 ± 0.003	1.04	10.8 ± 0.1	1.7 ± 0.4	0.16 ± 0.01
1531	GA3	195 ± 40	221 ± 40	192 ± 32	1.02 ± 0.004	1.04	10.5 ± 0.2	1.6 ± 0.3	0.15 ± 0.01
1532	GA4	146 ± 13	173 ± 24	146 ± 17	1.02 ± 0.01	1.02	12.5 ± 0.3	2.3 ± 0.3	0.15 ± 0.01
1533	GA5	194 ± 48	224 ± 57	186 ± 50	1.0 ± 0.2	1.04	10.5 ± 0.4	2.2 ± 0.6	0.16 ± 0.01
1403	GsF1	107 ± 6	112 ± 6	99 ± 6	1.1 ± 0.3	0.95	9.1 ± 0.4	4.2 ± 0.4	0.17 ± 0.02
1404	GsF2	69 ± 1	72 ± 1	62 ± 2	0.97 ± 0.00	0.97	9.4 ± 0.15	6.7 ± 0.1	0.5 ± 0.02

Table VII. Weighted fit values of the permeability μ_{33} for measurements taken under a compressive stress of –82.7 MPa. See Table VI for a description of the column headers.

NSWC ID	Sample ID	Fit Peak μ_{33} (nm / A)	Data Peak μ_{33} (nm / A)	20 – 80% μ_{33} (nm / A)	Fractional Amplitude	Avg Frac Amp	Center (kA/m)	Width (kA/m)	H_{shift} (kA/m)
1271	GF1	174 ± 72	184 ± 70	160 ± 71	1.02 ± 0.01	1.13	17.0 ± 0.2	2.56 ± 0.9	0.12 ± 0.01
1402	GF2	79 ± 9	98 ± 9	85 ± 6	1.02 ± 0.003	1.03	18.4 ± 1.3	3.4 ± 0.5	0.11 ± 0.01
1529	GA1	108 ± 18	133 ± 12	110 ± 14	1.02 ± 0.003	1.03	18.1 ± 0.7	2.8 ± 0.4	0.15 ± 0.01
1530	GA2	138 ± 25	160 ± 28	142 ± 23	1.03 ± 0.01	1.04	16.2 ± 0.2	2.1 ± 0.5	0.16 ± 0.01
1531	GA3	151 ± 31	172 ± 31	152 ± 28	1.03 ± 0.01	1.05	16.0 ± 0.3	1.9 ± 0.4	0.15 ± 0.01
1532	GA4	107 ± 11	131 ± 22	106 ± 13	1.03 ± 0.01	1.04	18.1 ± 0.5	3.0 ± 0.4	0.15 ± 0.01
1533	GA5	151 ± 60	172 ± 68	144 ± 58	1.02 ± 0.01	1.10	15.8 ± 0.5	2.8 ± 0.9	0.16 ± 0.01
1403	GsF1	88 ± 6	91 ± 6	82 ± 7	0.97 ± 0.01	0.97	13.6 ± 0.8	4.7 ± 0.9	0.17 ± 0.02
1404	GsF2	58.4 ± 0.9	59 ± 1	52 ± 1	0.98 ± 0.001	0.98	13.7 ± 0.3	7.7 ± 0.2	0.25 ± 0.04

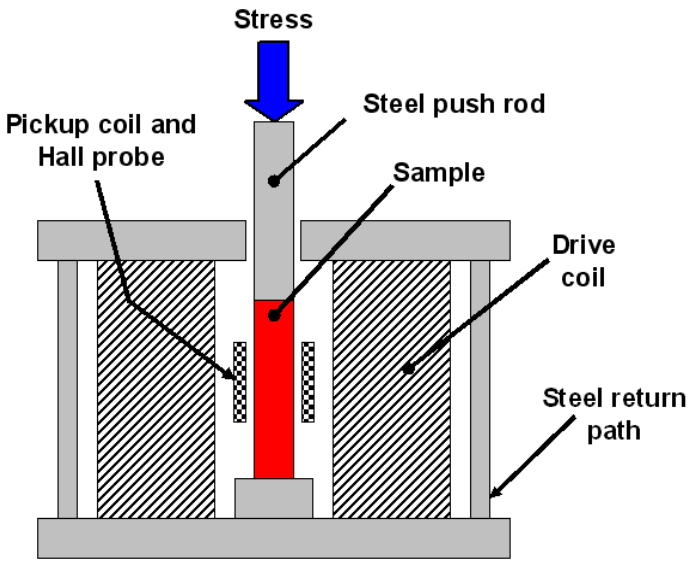

Figure 1. Schematic of the experimental test apparatus.

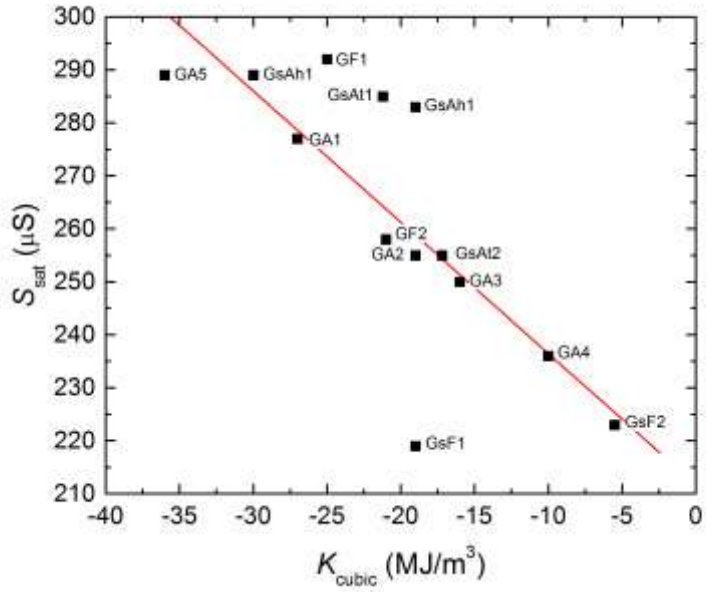

Figure 2. A linear fit $y = S_{sat} = m\,K_{cubic} + b$ between S_{sat} and the fit parameter K_{cubic} for the Galfenol (G) and Galfenol steel (Gs) samples; $m = -2.5 \pm 0.6$, $b = 212 \pm 13$ and $R = -0.77$.

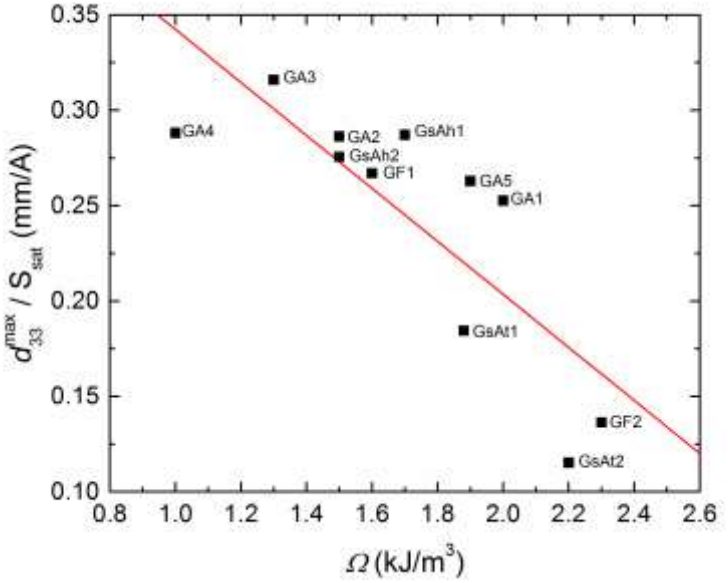

Figure 3. A linear fit $y = d_{33} / S_{sat} = m\Omega + b$ between d_{33} / S_{sat} and the fit parameter Ω for the Galfenol (G) and Galfenol steel (Gs) samples; $m = -0.14 \pm 0.03$, $b = 0.48 \pm 0.1$ and $R = -0.81$.

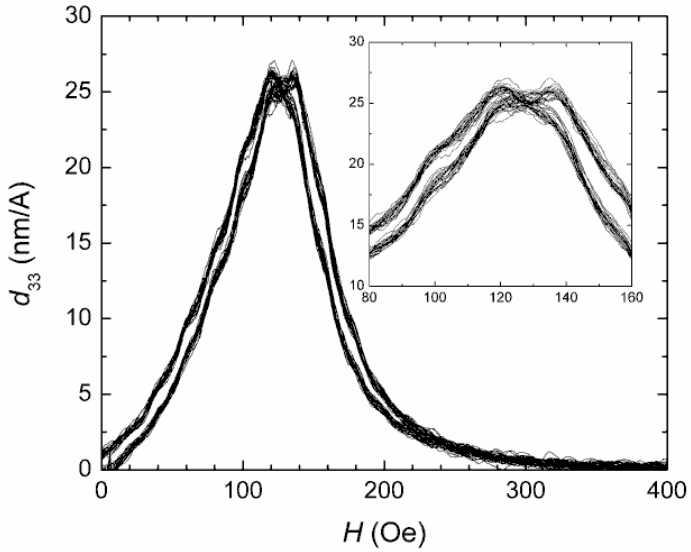

Figure 4. Ten repeated measurements of the piezomagnetic constant d_{33} on sample GsF1 during a single mounting of the sample in the experimental test apparatus at a stress of –55.2 MPa. The inset shows the detail around the peak d_{33}.

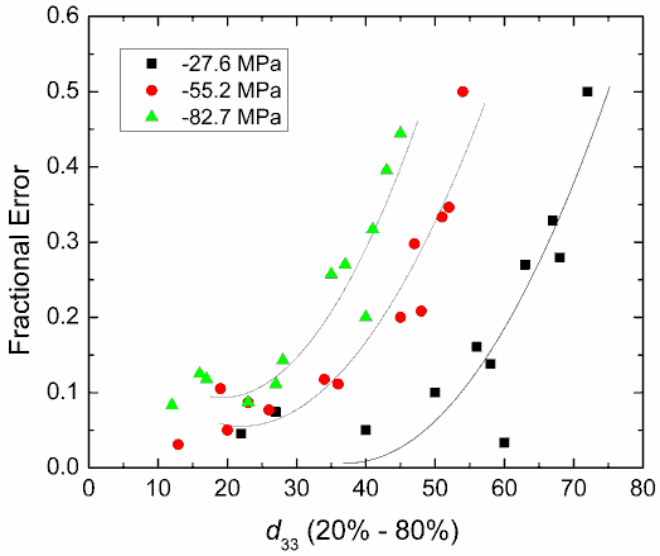

Figure 5. The relationship between d_{33} (20% to 80%) and its fractional error for Galfenol (G) and Galfenol Steel (Gs) samples at stresses of –27.6, –55.2 and –82.7 MPa. The curves show that the samples with higher d_{33} have more variation due to sample mounting. The curves are initially flat and then increase in a parabolic fashion. The solid lines are best-fit parabolas to the increasing part of the data sets.

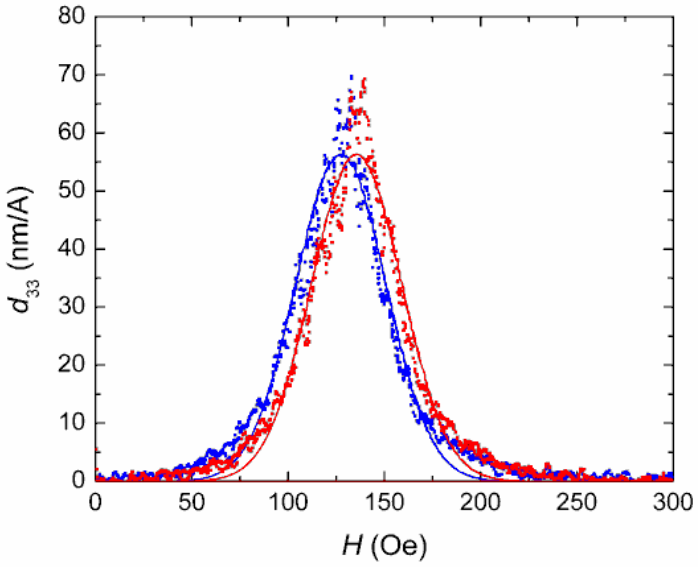

Figure 6. Measurements of the piezomagnetic constant d_{33} for sample GA5 at –55.2 MPa. Also shown are fits for d_{33} for both the up and down field directions.

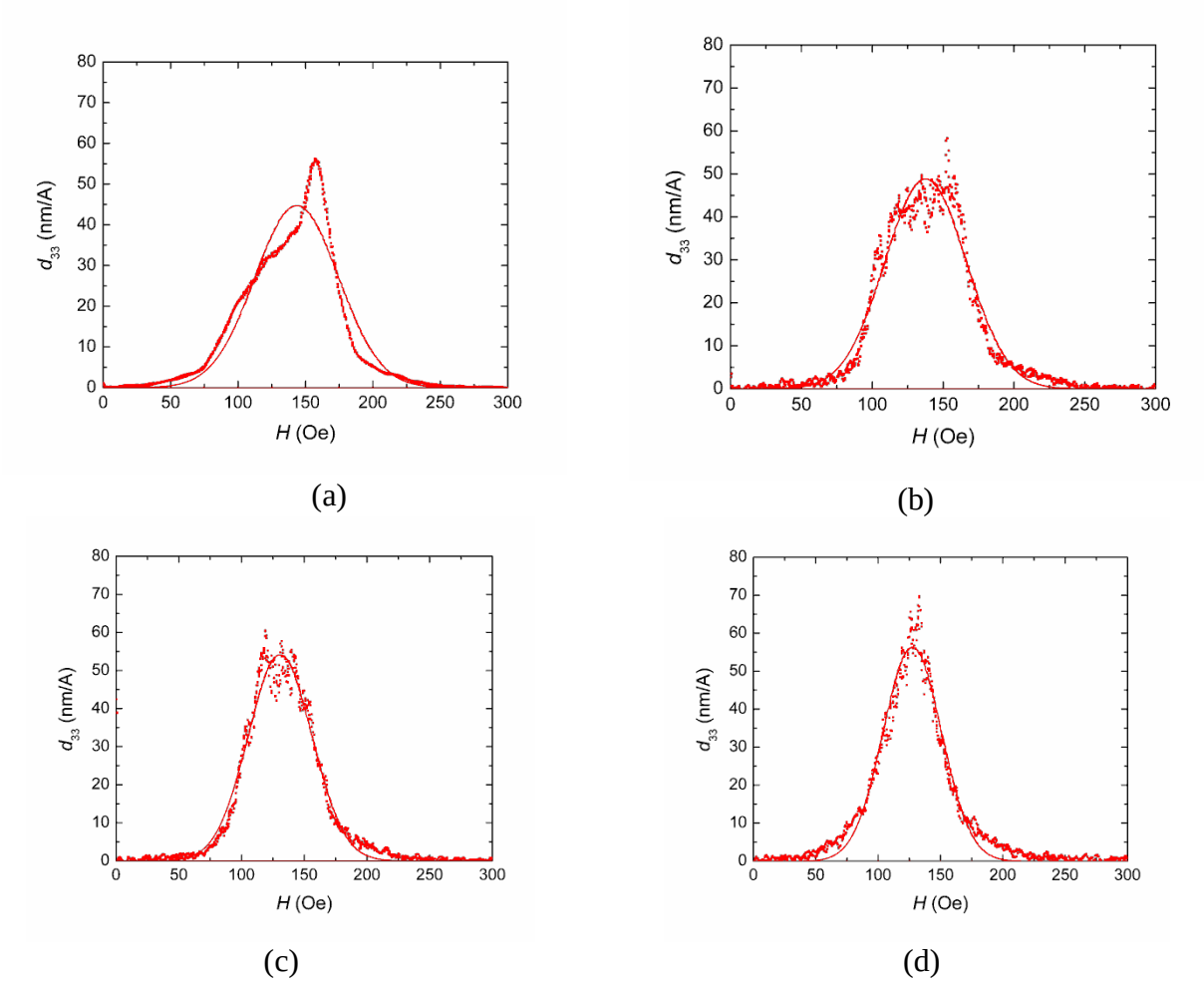

Figure 7. The piezomagnetic constant d_{33} for sample GA5 at –55.2 MPa showing the measurements and fit results for increasing H for the last four mountings of the sample in the experimental test apparatus.

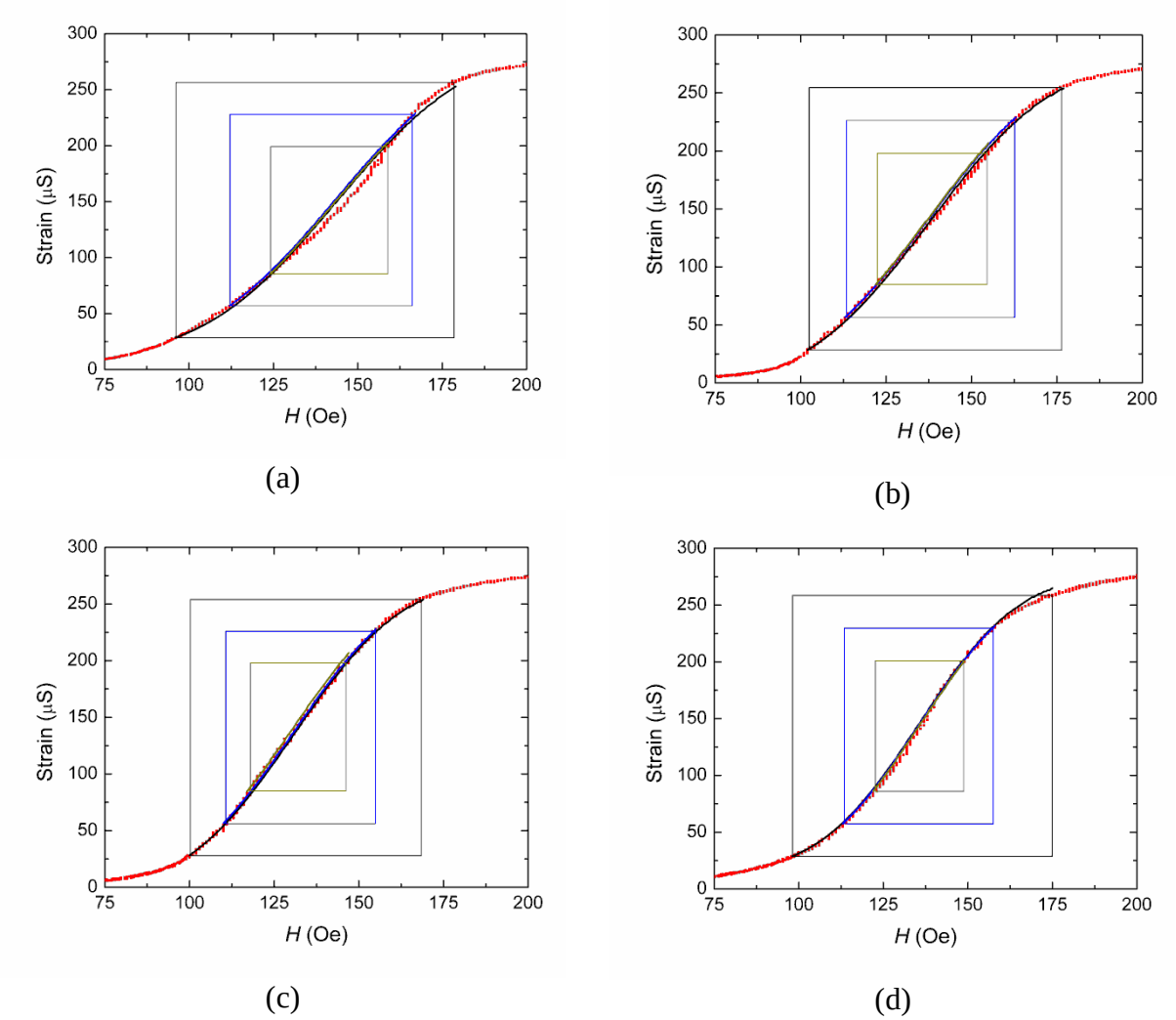

Figure 8. Strain S derived from the fitted d_{33} for Sample GA5 at –55.2 MPa from the measurements taken for the last four mountings of the sample in the experimental test apparatus. The three boxes represent the strain ranges from 10 to 90 percent, 20 to 80 percent, and 30 to 70 percent of S_{sat}. The corresponding fit results for these ranges are indicated on the graphs.

This page intentionally left blank

APPENDIX A – Galfenol ($Fe_{81.6}Ga_{18.4}$) FSZM Samples

Sample GF1:

- Magnetostriction *S* and magnetization *B* as a function of magnetic field *H* under compressive stresses of –13.8, –27.6, –41.4, –55.2, –69.0, –82.7, and –96.5 MPa.

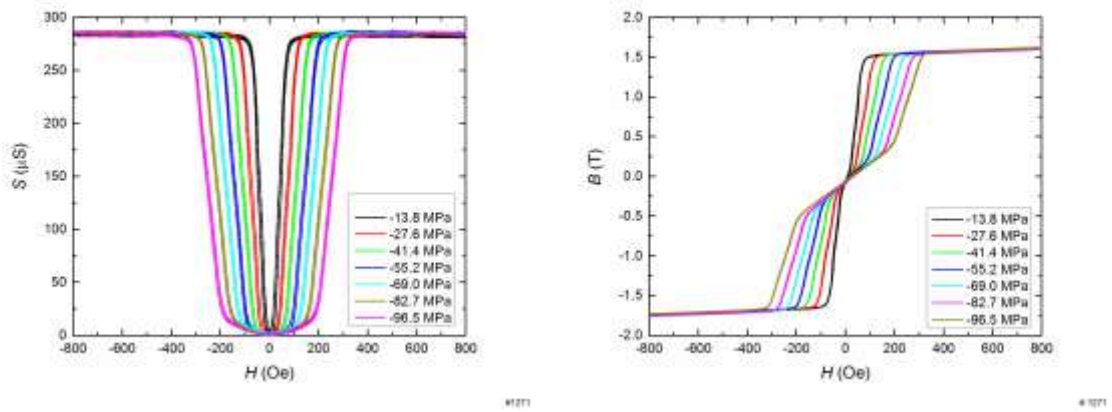

- Piezomagnetic constants d_{33} and relative permeability μ_{33} as a function of magnetic field *H* under compressive stresses of –13.8, –27.6, –41.4, –55.2, –69.0, –82.7, and –96.5 MPa.

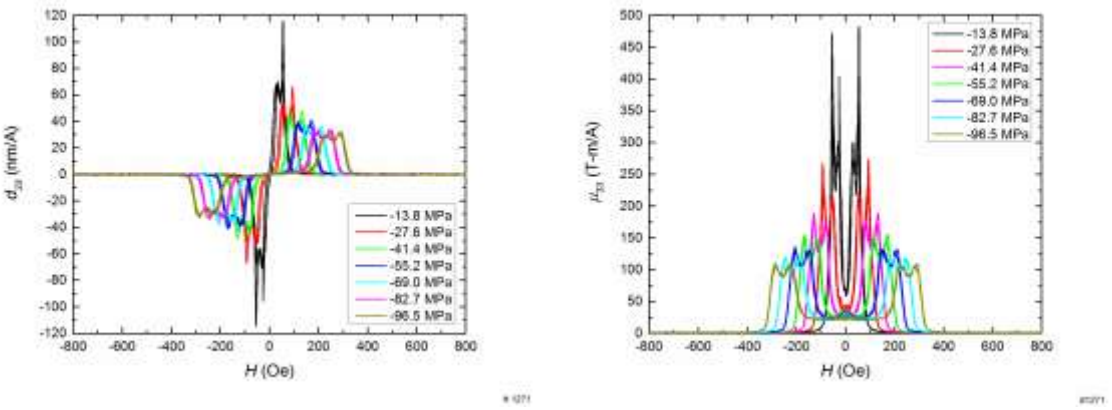

- constant stress of –55.2 MPa for repeated mountings in the experimental apparatus

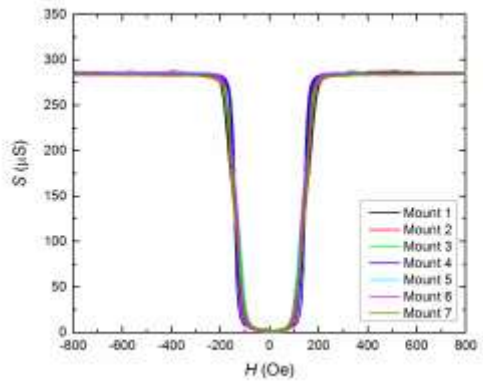

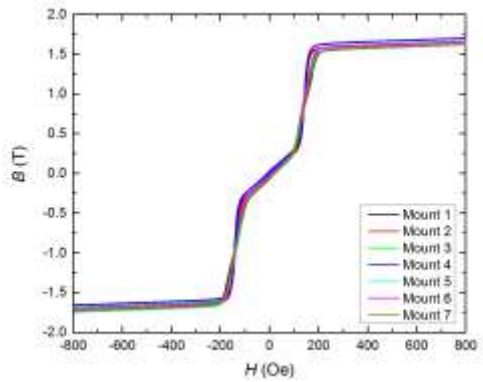

- Piezomagnetic constant d_{33} and relative permeability μ_{33} as a function of magnetic field H under a constant stress of –55.2 MPa for repeated mountings in the experimental apparatus

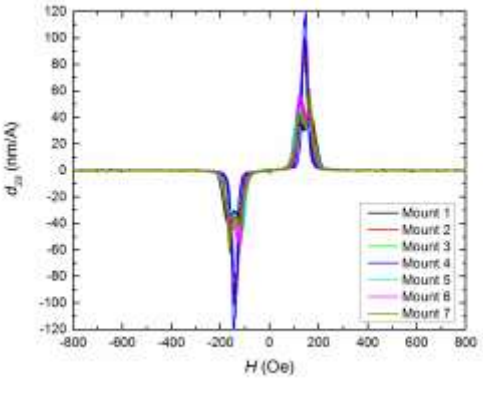

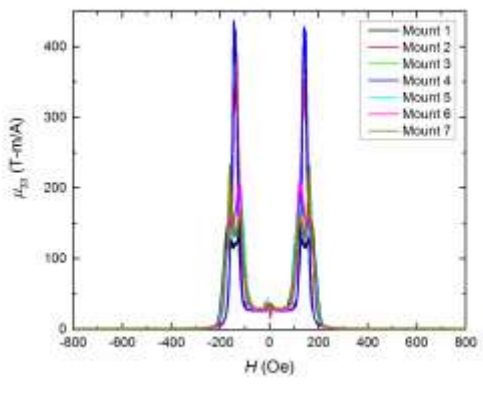

Sample GF2:

- Magnetostriction *S* and magnetization *B* as a function of magnetic field *H* under compressive stresses of –27.6, –41.4, –55.2, –69.0, –82.7, –96.5, and –124.1 MPa.

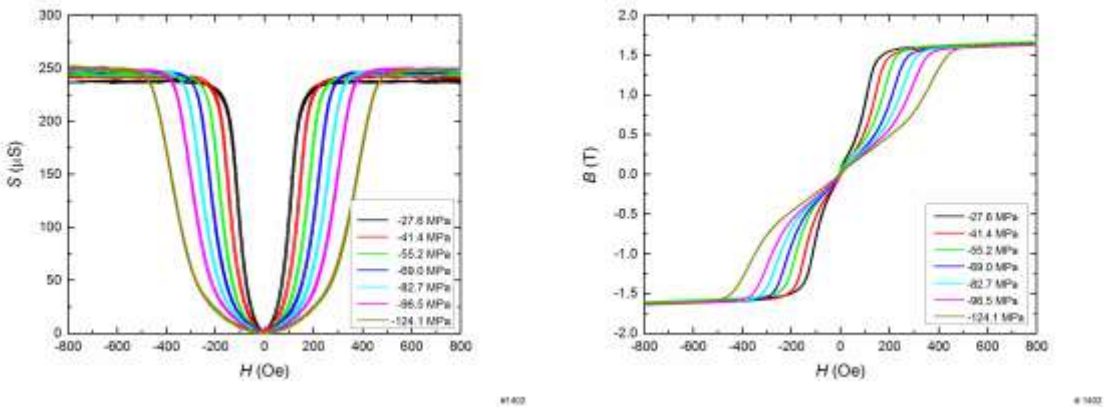

- Piezomagnetic constants d_{33} and relative permeability μ_{33} as a function of magnetic field *H* under compressive stresses of —27.6, –41.4, –55.2, –69.0, –82.7, –96.5, and –124.1 MPa.

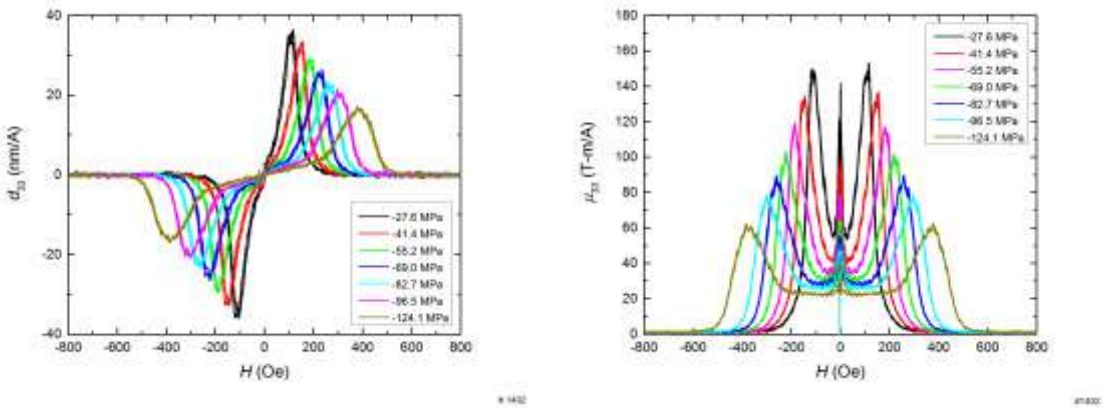

- Strain *S* and magnetization *B* as a function of stress *T* for magnetic fields of 151, 200, 250, and 301 Oe.

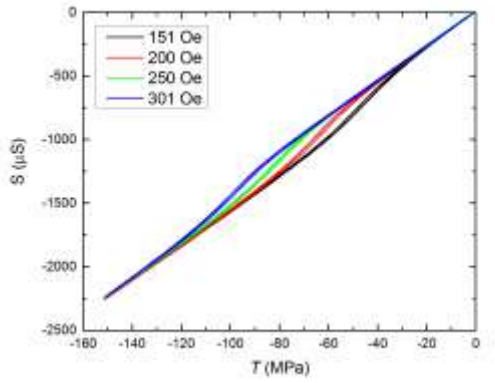

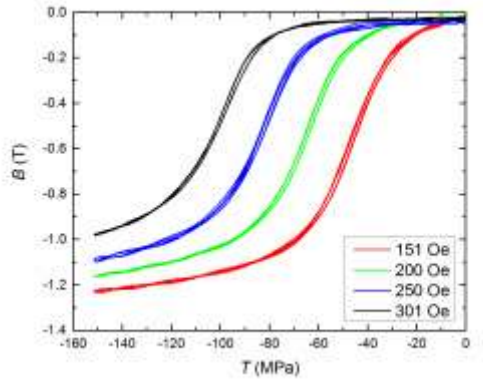

- Piezomagnetic constant d_{33}* and modulus *E* as a function of stress *T* for magnetic fields of 151, 200, 250, and 301 Oe.

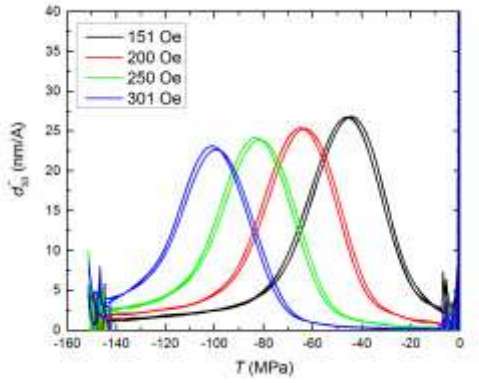

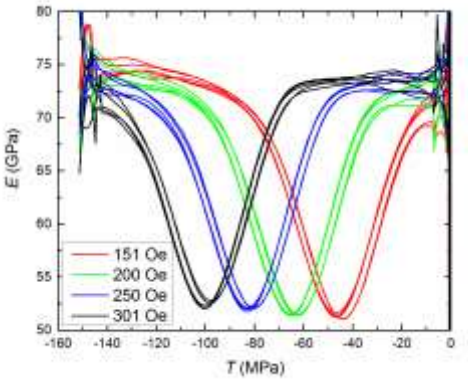

- Magnetostriction *S* and magnetization *B* as a function of magnetic field *H* under a constant stress of –55.2 MPa for repeated mountings in the experimental apparatus

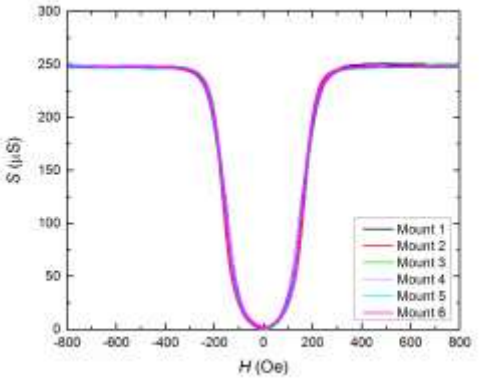

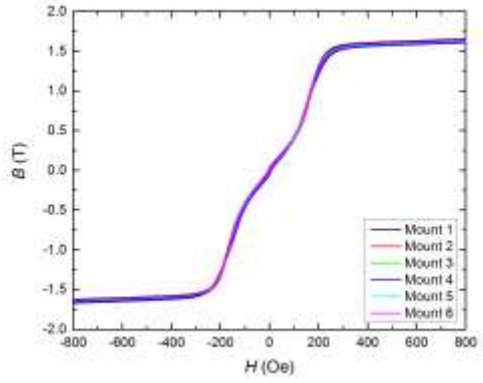

- Piezomagnetic constant d_{33} and relative permeability μ_{33} as a function of magnetic field H under a constant stress of –55.2 MPa for repeated mountings in the experimental apparatus

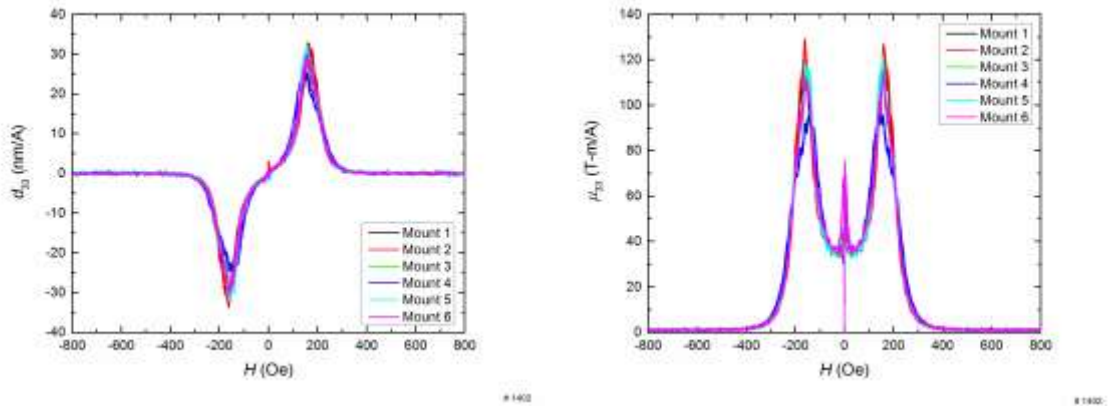

APPENDIX B – Galfenol ($Fe_{81.6}Ga_{18.4}$) Advanced Bridgman Samples

Sample GA1:

- Magnetostriction *S* and magnetization *B* as a function of magnetic field *H* under compressive stresses of –13.8, –41.4,–69.0, –96.6, and –151.7 MPa.

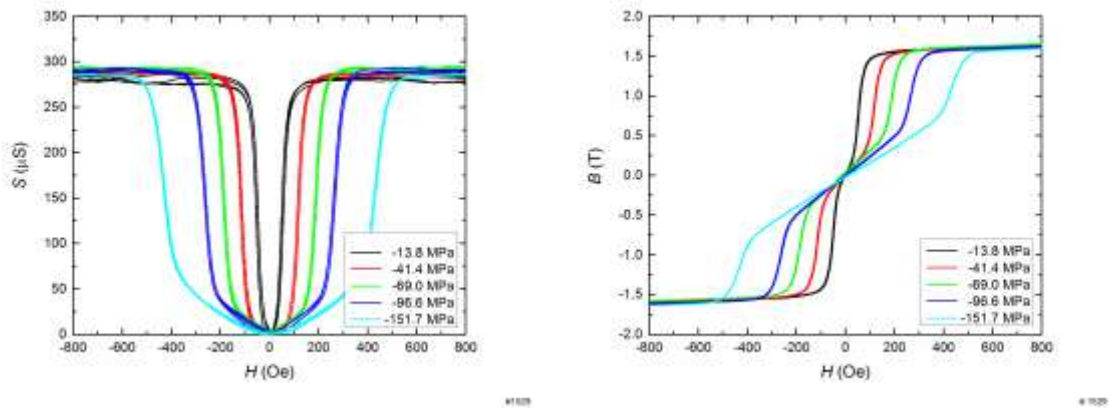

- Piezomagnetic constants d_{33} and relative permeability μ_{33} as a function of magnetic field *H* under compressive stresses of –13.8, –41.4,–69.0, –96.6, and –151.7 MPa.

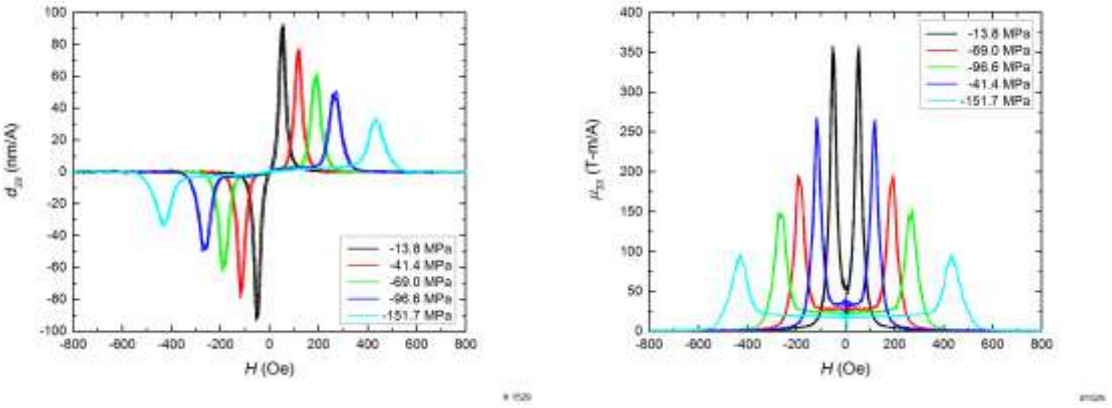

- Strain *S* and magnetization *B* as a function of stress *T* for magnetic fields of 149, 249, and 349 Oe.

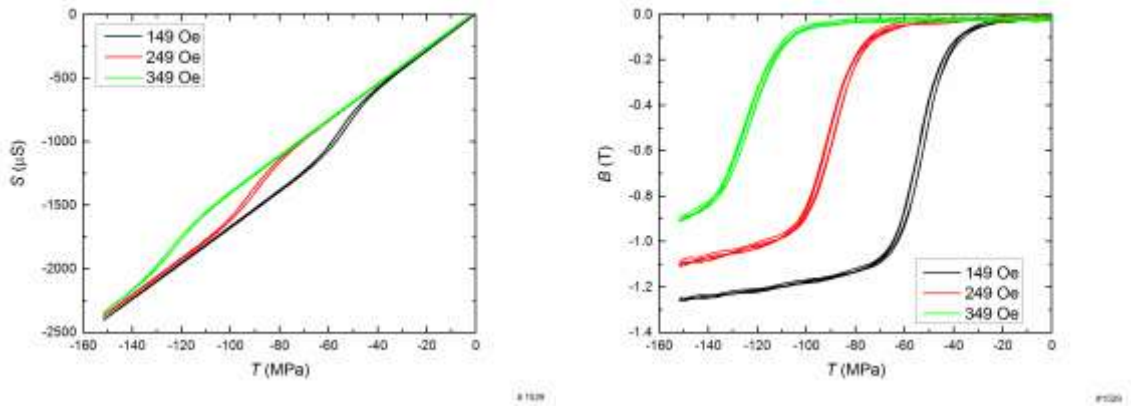

- Piezomagnetic constant d_{33}* and modulus *E* as a function of stress *T* for magnetic fields of 149, 249, and 349 Oe.

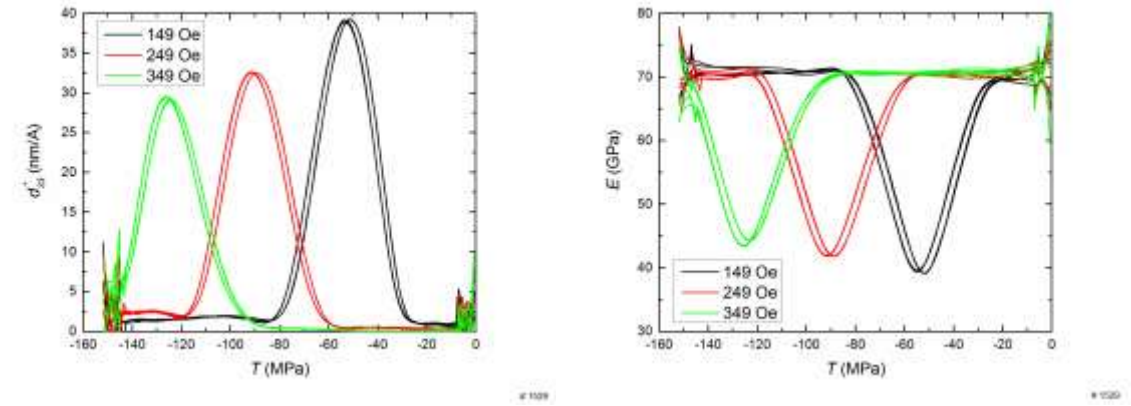

- Magnetostriction *S* and magnetization *B* as a function of magnetic field *H* under a constant stress of –55.2 MPa for repeated mountings in the experimental apparatus

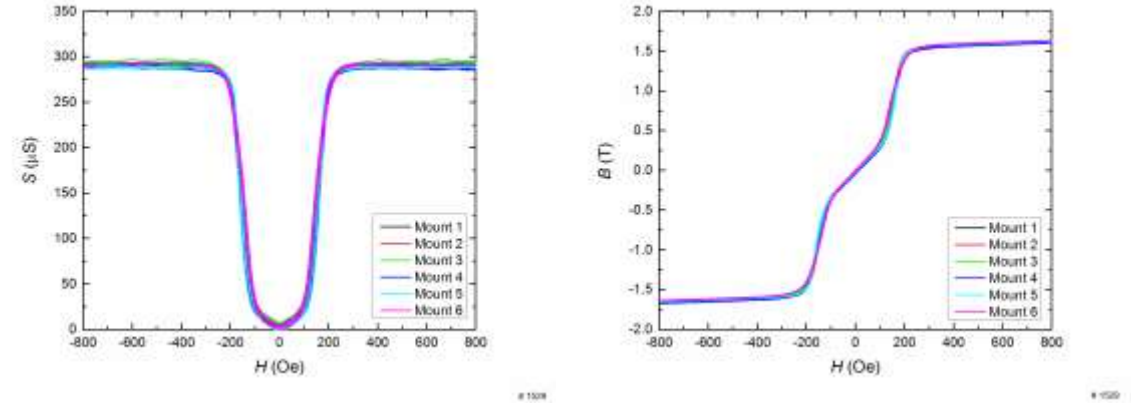

- Piezomagnetic constant d_{33} and relative permeability μ_{33} as a function of magnetic field H under a constant stress of –55.2 MPa for repeated mountings in the experimental apparatus

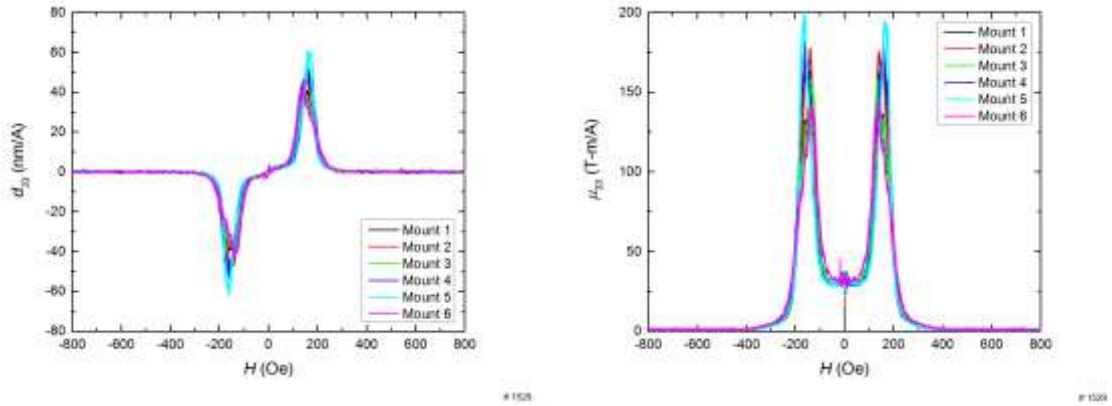

Sample GA2:

- Magnetostriction S and magnetization B as a function of magnetic field H under compressive stresses of –13.8,–41.4,–69.2,–98.6, and –152.2 MPa.

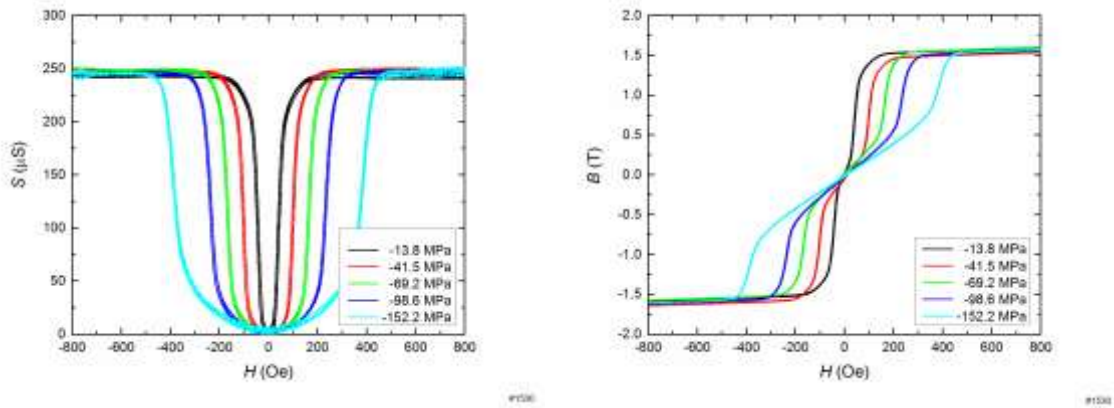

- Piezomagnetic constants d_{33} and relative permeability μ_{33} as a function of magnetic field H under compressive stresses of –13.8,–41.4,–69.2,–98.6, and –152.2 MPa.

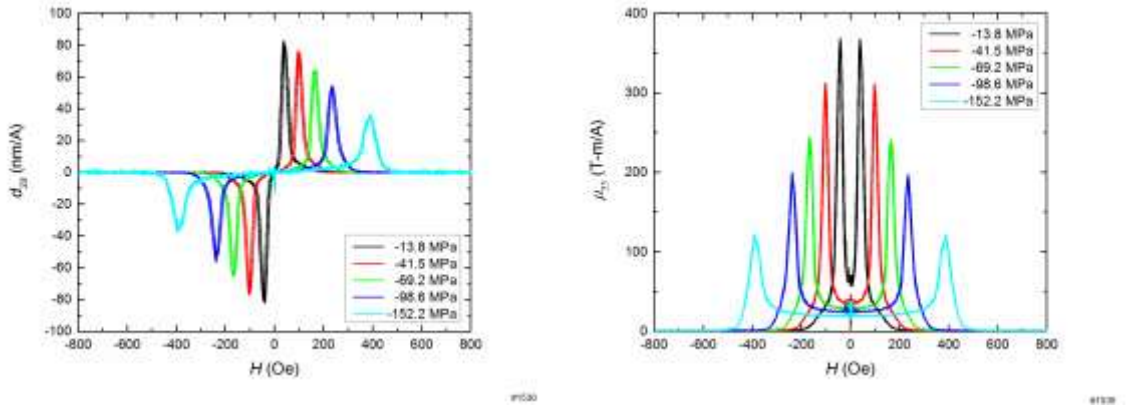

- Strain S and magnetization B as a function of stress T for magnetic fields of 96, 196, and 296 Oe.

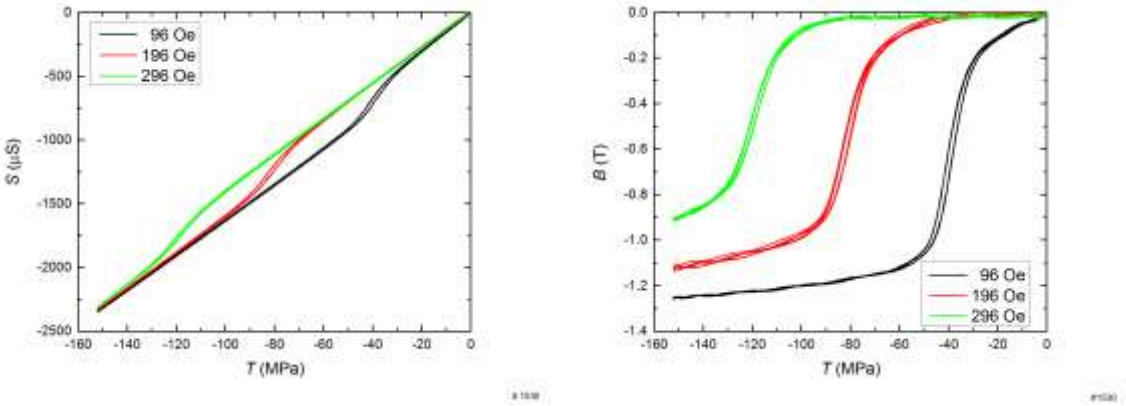

- Piezomagnetic constant d_{33}* and modulus E as a function of stress T for magnetic fields of 96, 196, and 296 Oe.

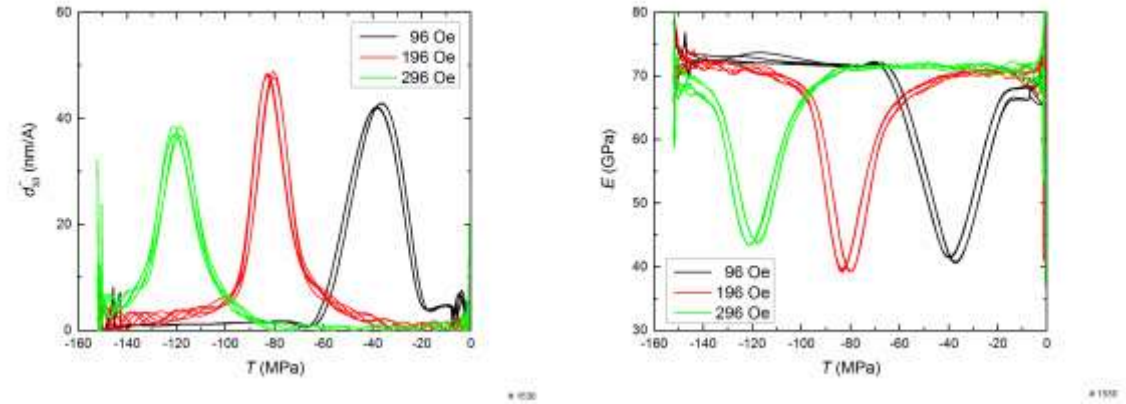

- Magnetostriction S and magnetization B as a function of magnetic field H under a constant stress of –55.2 MPa for repeated mountings in the experimental apparatus

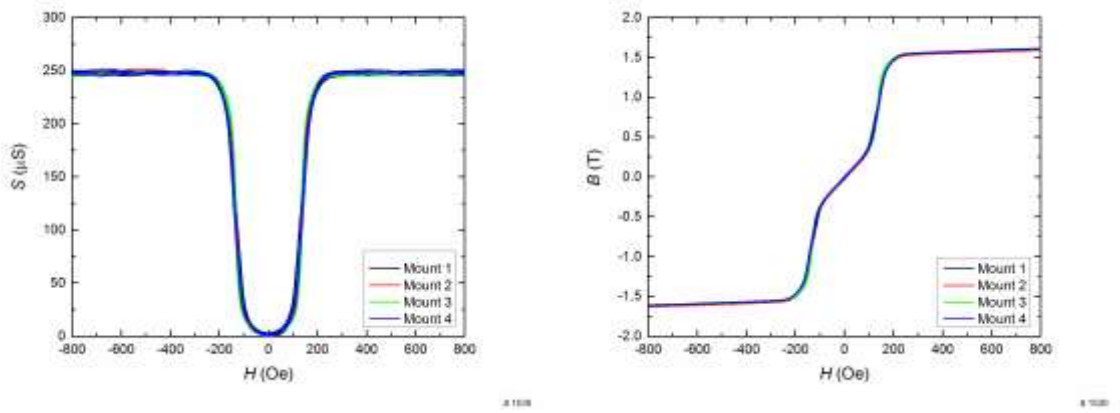

- Piezomagnetic constant d_{33} and relative permeability μ_{33} as a function of magnetic field H under a constant stress of –55.2 MPa for repeated mountings in the experimental apparatus

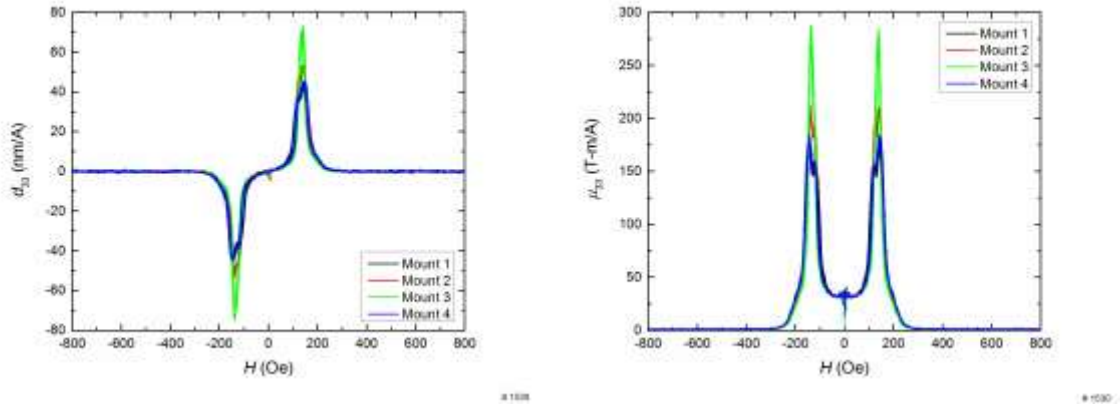

Sample GA3:

- Magnetostriction *S* and magnetization *B* as a function of magnetic field *H* under compressive stresses of –13.8, –27.6, –41.4,–69.0, and –96.5 MPa.

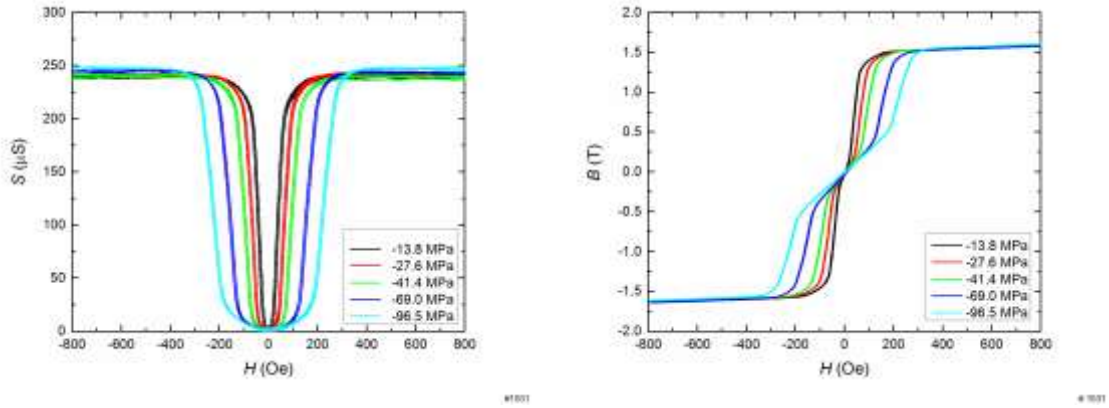

- Piezomagnetic constants d_{33} and relative permeability μ_{33} as a function of magnetic field *H* under compressive stresses of –13.8, –27.6, –41.4,–69.0, and –96.5 MPa.

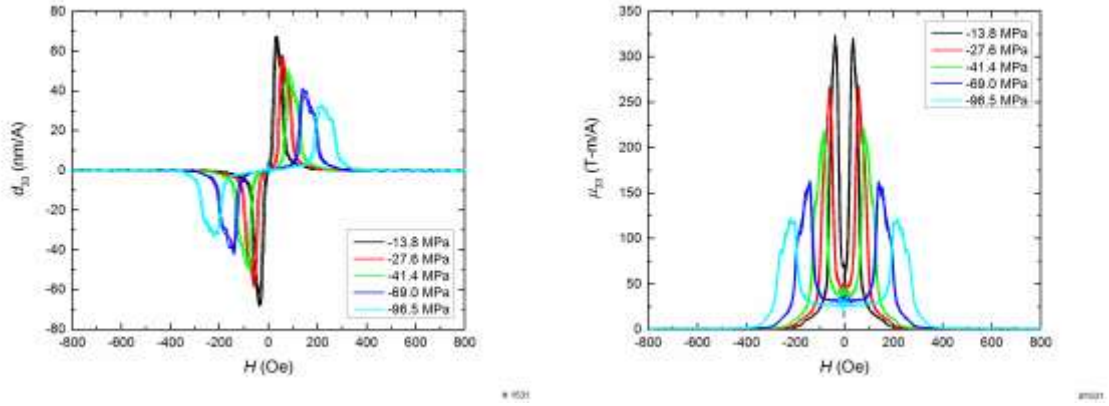

- Strain *S* and magnetization *B* as a function of stress *T* for magnetic fields of 75, 100, and 125 Oe.

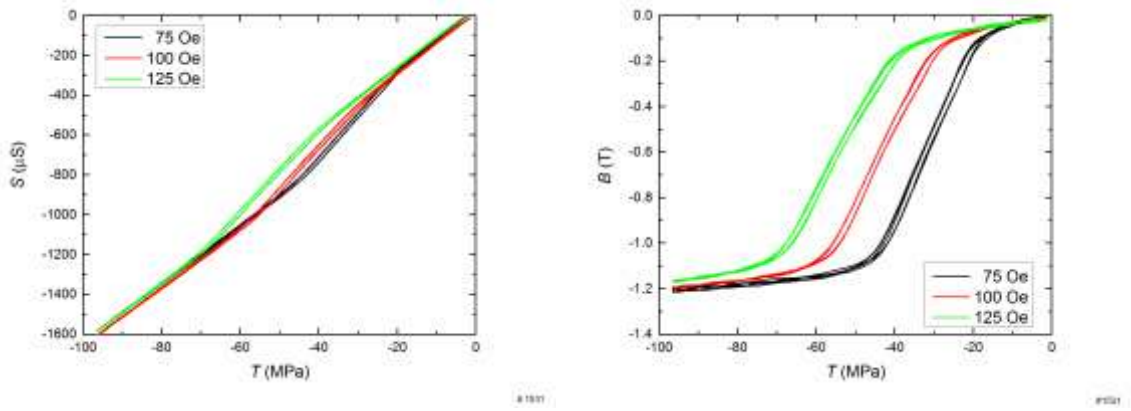

- Piezomagnetic constant d_{33}* and modulus *E* as a function of stress *T* for magnetic fields of 75, 100, and 125 Oe.

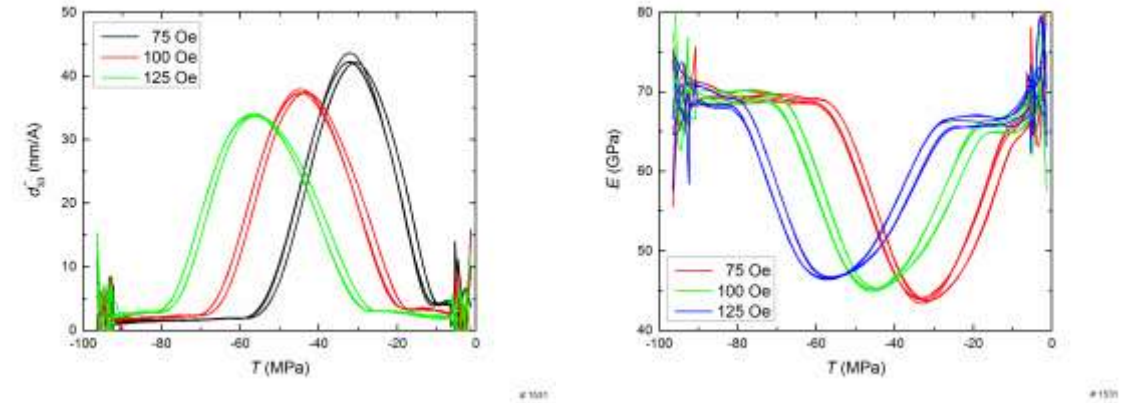

- Magnetostriction *S* and magnetization *B* as a function of magnetic field *H* under a constant stress of –55.2 MPa for repeated mountings in the experimental apparatus

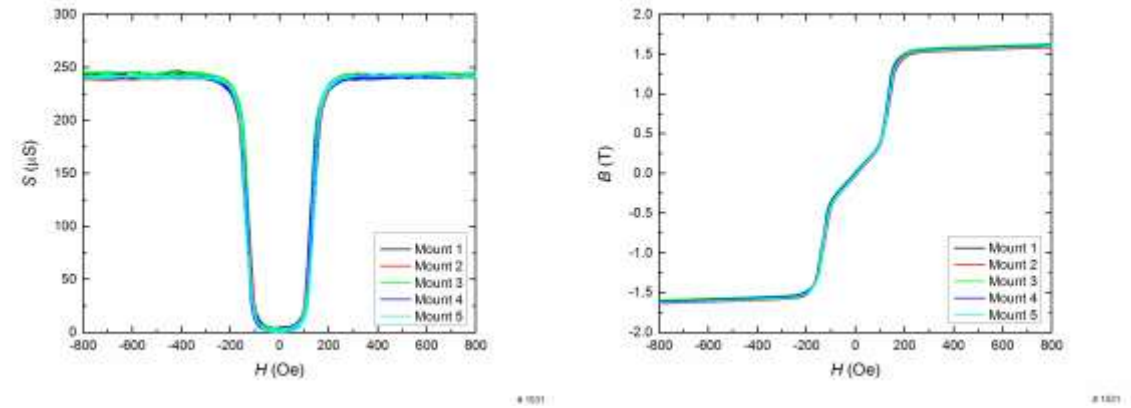

- Piezomagnetic constant d_{33} and relative permeability μ_{33} as a function of magnetic field H under a constant stress of –55.2 MPa for repeated mountings in the experimental apparatus

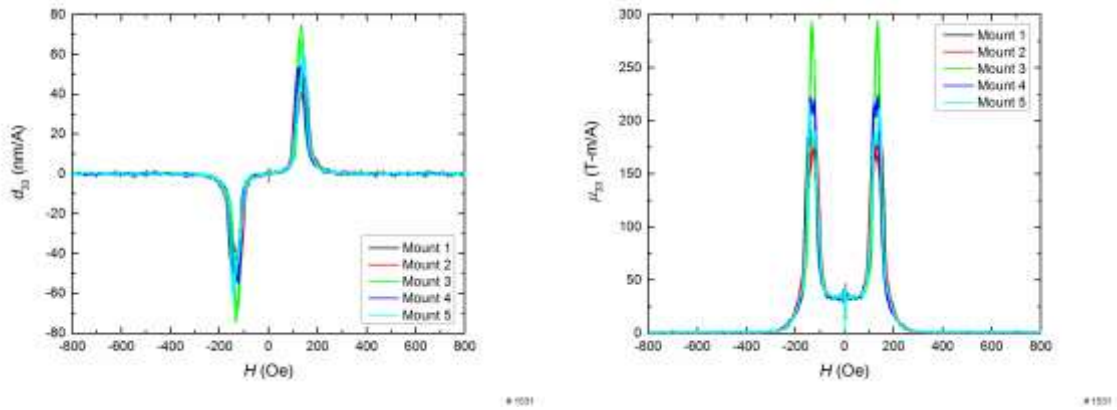

Sample GA4:

- Magnetostriction S and magnetization B as a function of magnetic field H under compressive stresses of –13.7, –27.5, –41.2,–68.7, and –96.1 MPa.

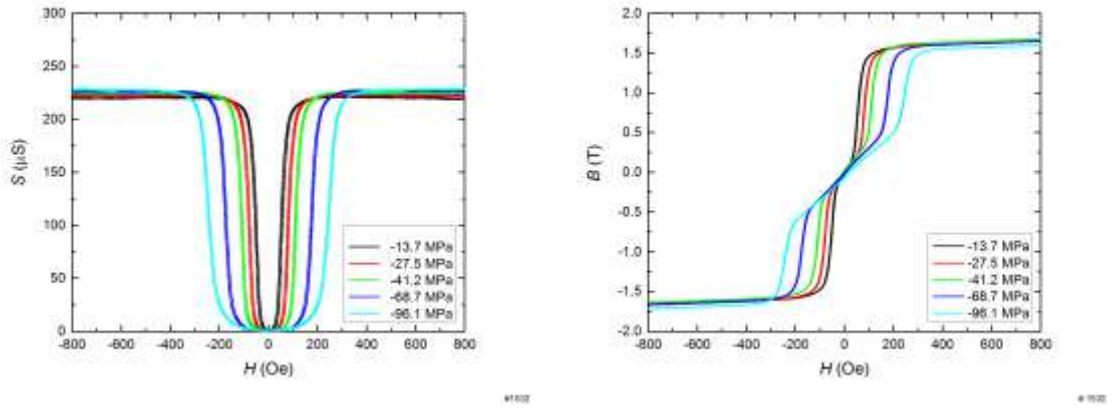

- Piezomagnetic constants d_{33} and relative permeability μ_{33} as a function of magnetic field H under compressive stresses of –13.7, –27.5, –41.2,–68.7, and –96.1 MPa.

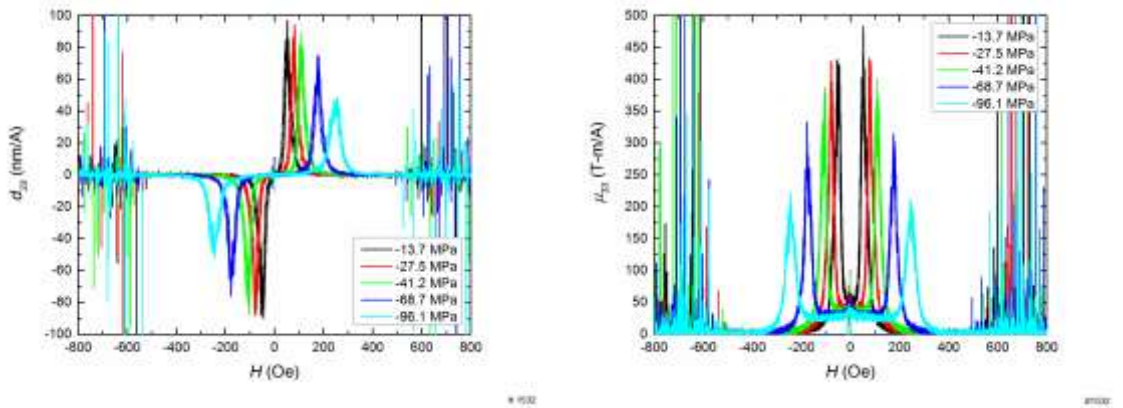

- Strain *S* and magnetization *B* as a function of stress *T* for magnetic fields of 100, 125, 150, and 175 Oe.

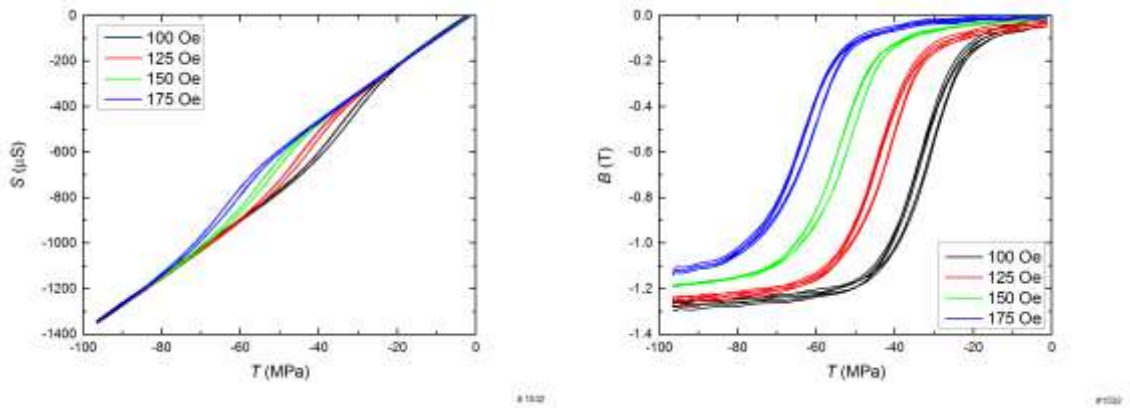

- Piezomagnetic constant d_{33}* and modulus *E* as a function of stress *T* for magnetic fields of 100, 125, 150, and 175 Oe.

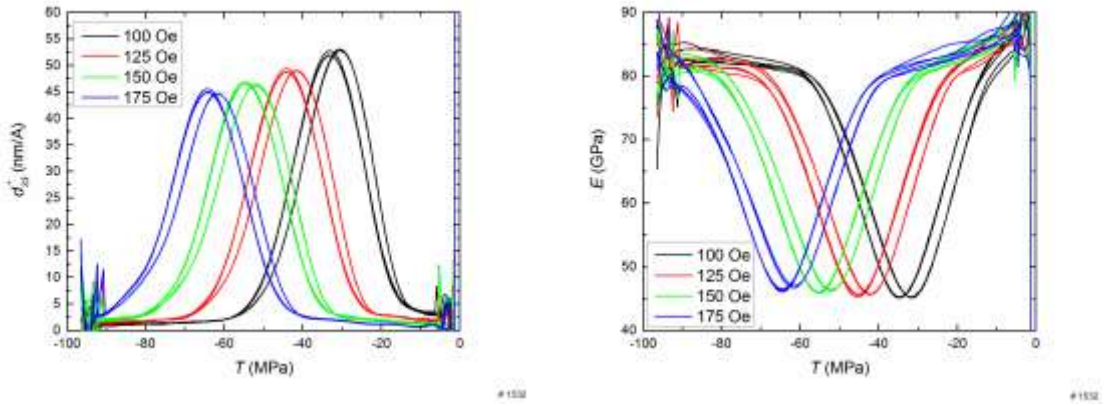

- Magnetostriction *S* and magnetization *B* as a function of magnetic field *H* under a constant stress of –55.2 MPa for repeated mountings in the experimental apparatus

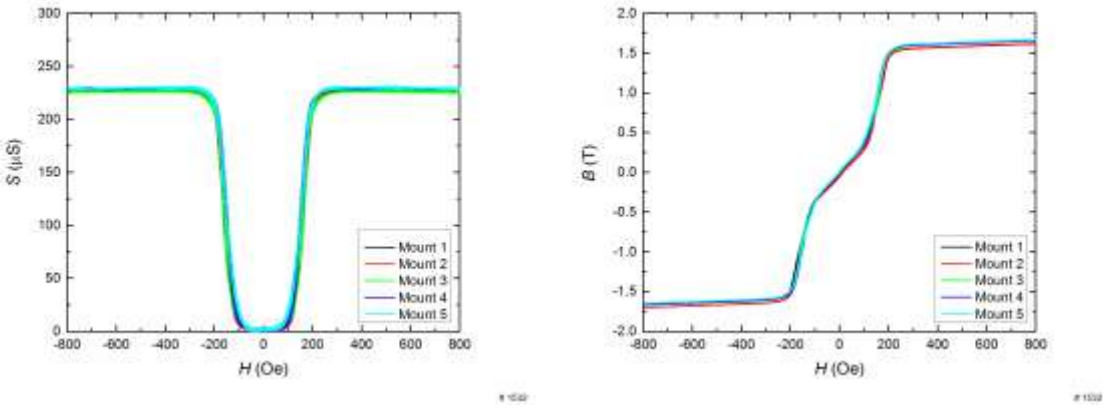

- Piezomagnetic constant d_{33} and relative permeability μ_{33} as a function of magnetic field H under a constant stress of –55.2 MPa for repeated mountings in the experimental apparatus

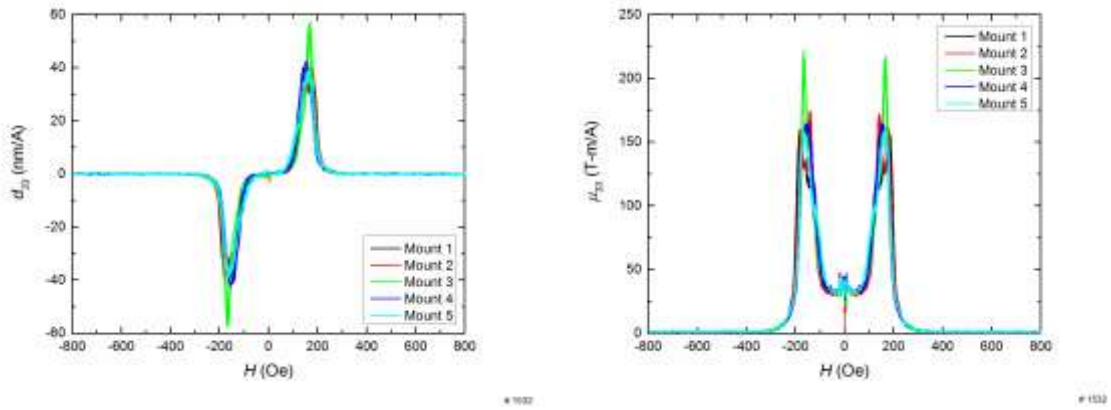

Sample GA5:

- Magnetostriction S and magnetization B as a function of magnetic field H under compressive stresses of –27.6, –41.4, –55.2, –69.0, –82.7, –96.5, and –124.1 MPa.

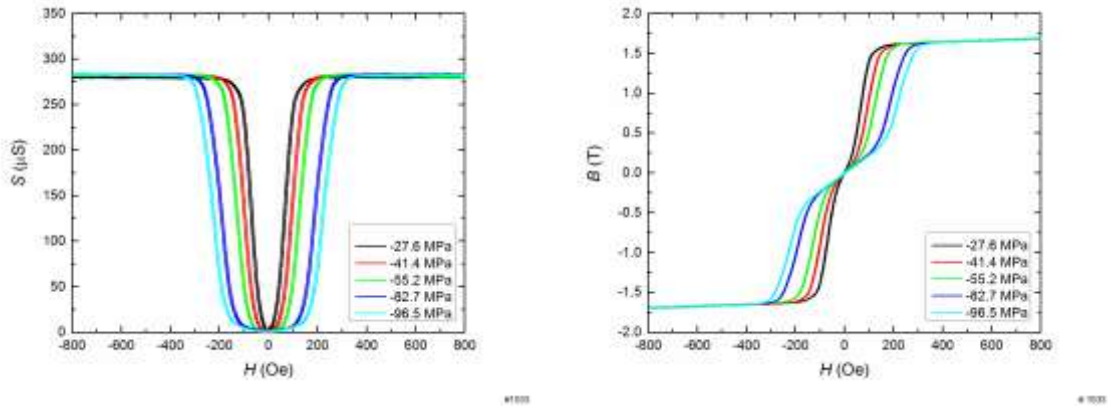

- Piezomagnetic constants d_{33} and relative permeability μ_{33} as a function of magnetic field H under compressive stresses of –27.6, –41.4, –55.2, –69.0, –82.7, –96.5, and –124.1 MPa.

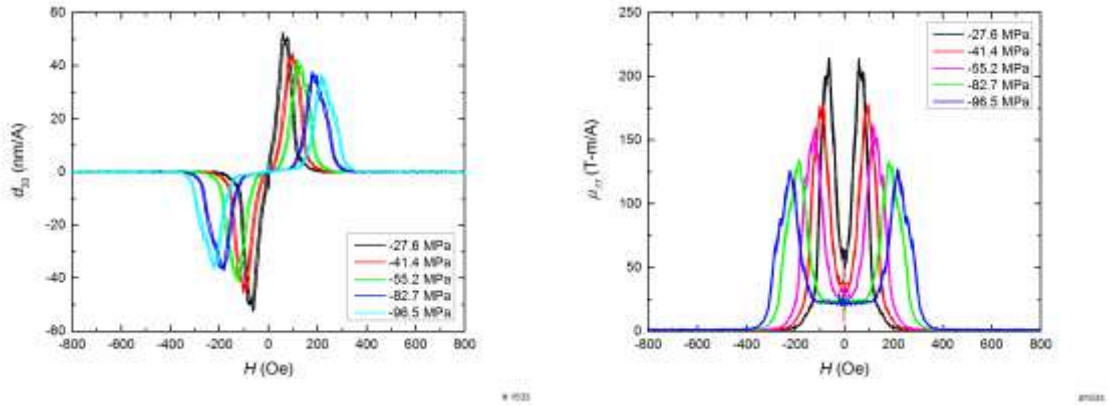

- Strain *S* and magnetization *B* as a function of stress *T* for magnetic fields of 75 and 100 Oe.

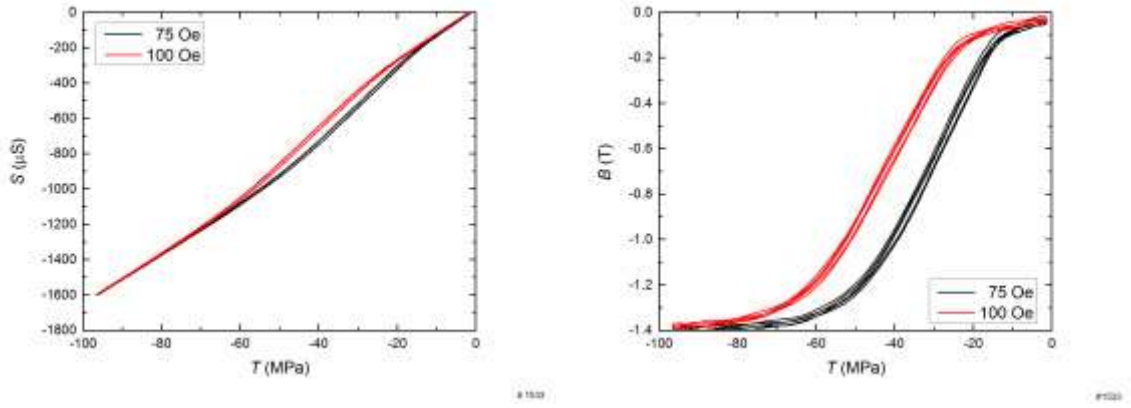

- Piezomagnetic constant d_{33}* and modulus *E* as a function of stress *T* for magnetic fields of 75 and 100 Oe.

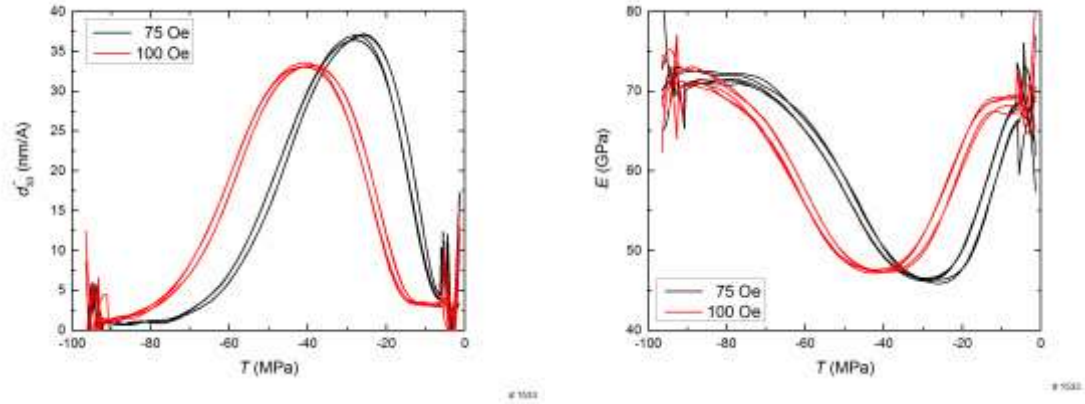

- Magnetostriction *S* and magnetization *B* as a function of magnetic field *H* under a constant stress of –55.2 MPa for repeated mountings in the experimental apparatus

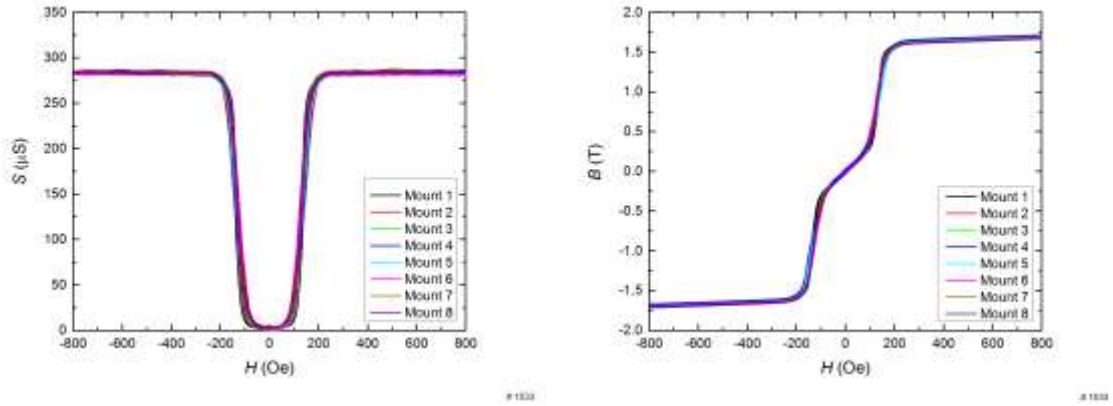

- Piezomagnetic constant d_{33} and relative permeability μ_{33} as a function of magnetic field *H* under a constant stress of –55.2 MPa for repeated mountings in the experimental apparatus

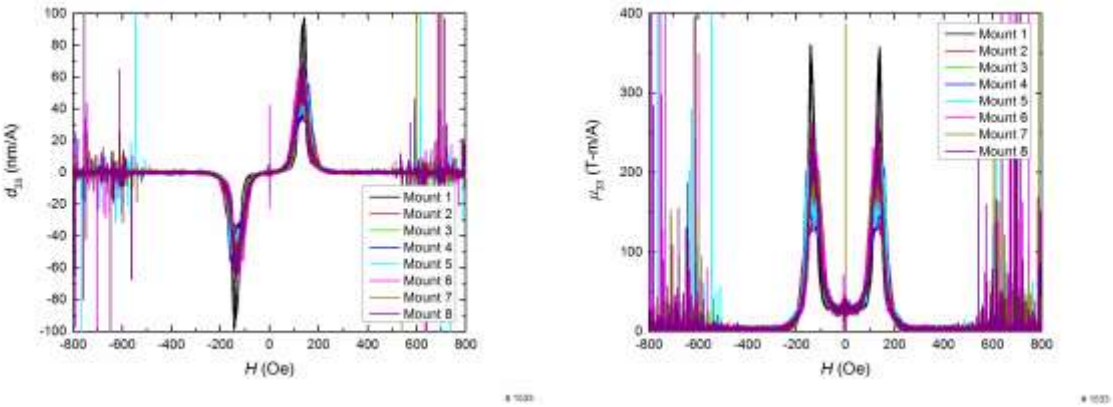

APPENDIX C – Galfenol Steel ($Fe_{81.6}Ga_{18.4}$ + C) FSZM Samples

Sample GsF1:

- Magnetostriction *S* and magnetization *B* as a function of magnetic field *H* under compressive stresses of –27.6, –41.4, –55.2, –69.0, and –96.5 MPa.

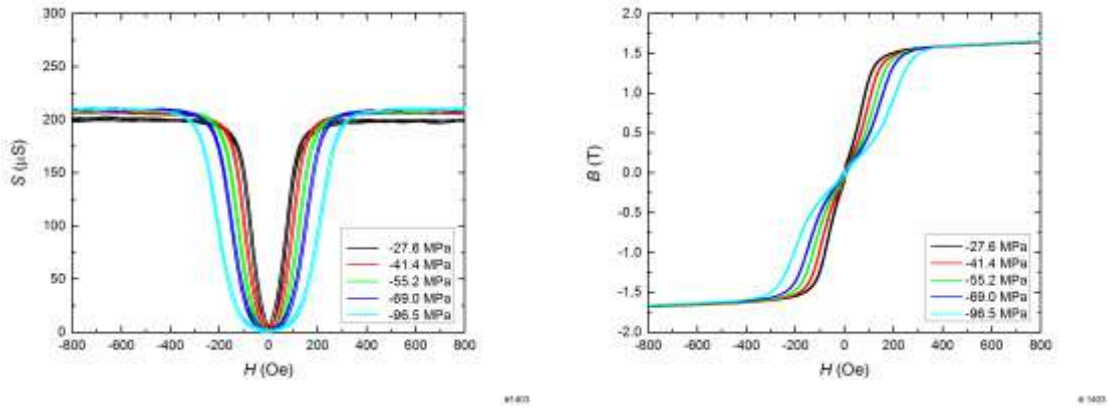

- Piezomagnetic constants d_{33} and relative permeability μ_{33} as a function of magnetic field *H* under compressive stresses of –27.6, –41.4, –55.2, –69.0, and –96.5 MPa.

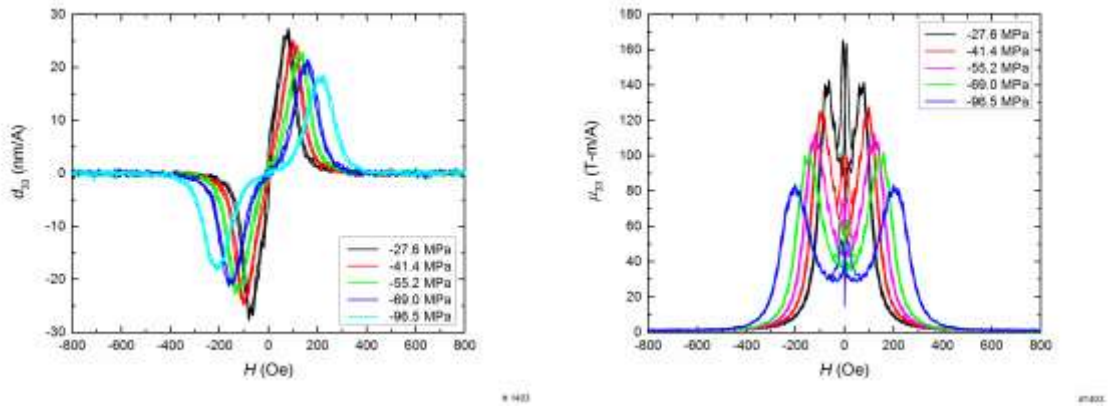

- Strain *S* and magnetization *B* as a function of stress *T* for magnetic fields of 125 and 150 Oe.

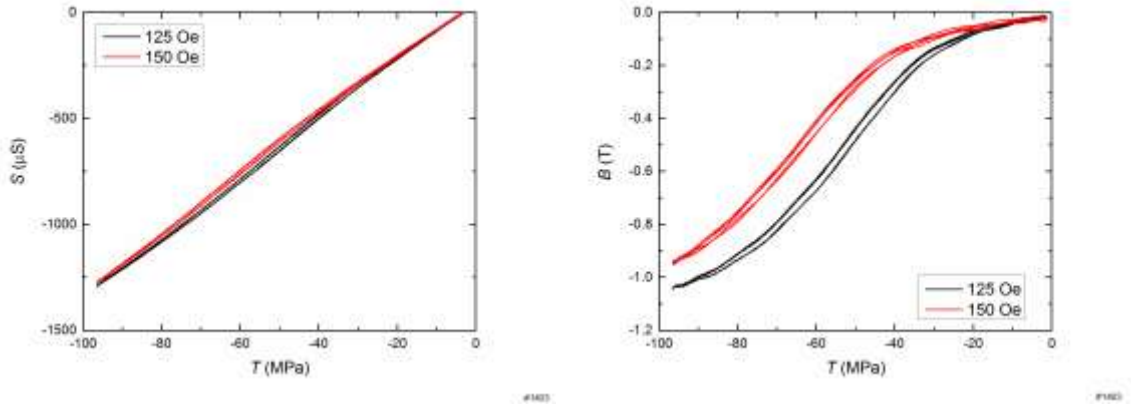

- Piezomagnetic constant d_{33}* and modulus *E* as a function of stress *T* for magnetic fields of 125 and 150 Oe.

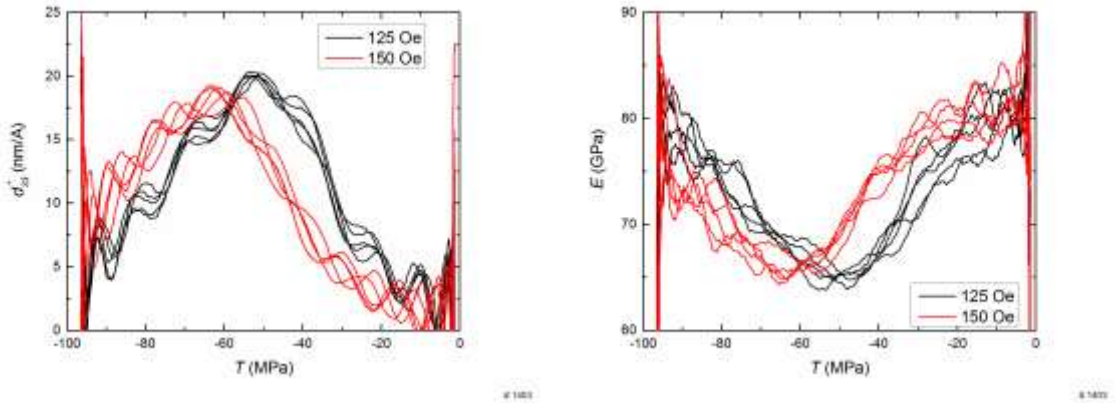

- Magnetostriction *S* and magnetization *B* as a function of magnetic field *H* under a constant stress of –55.2 MPa for repeated mountings in the experimental apparatus

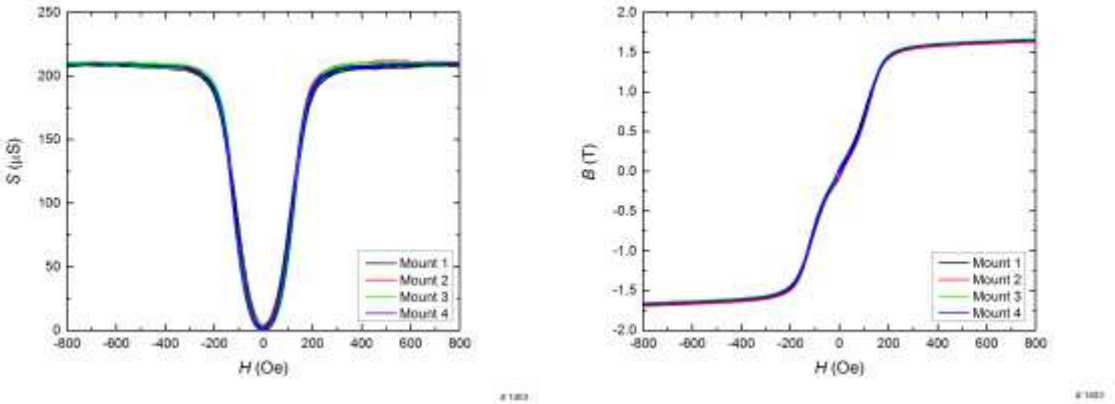

- Piezomagnetic constant d_{33} and relative permeability μ_{33} as a function of magnetic field *H* under a constant stress of –55.2 MPa for repeated mountings in the experimental apparatus

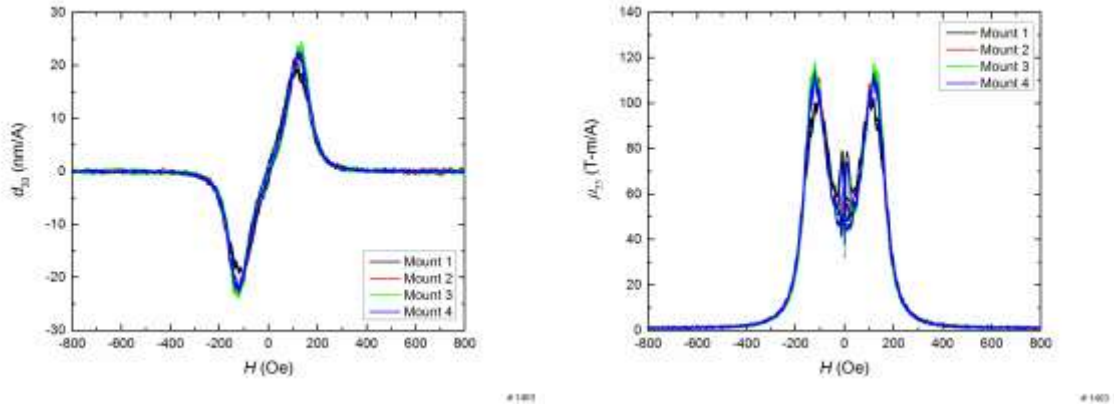

Sample GsF2:

- Magnetostriction *S* and magnetization *B* as a function of magnetic field *H* under compressive stresses of –55.0, –68.7, –82.5, –96.2, and –123.7 MPa.

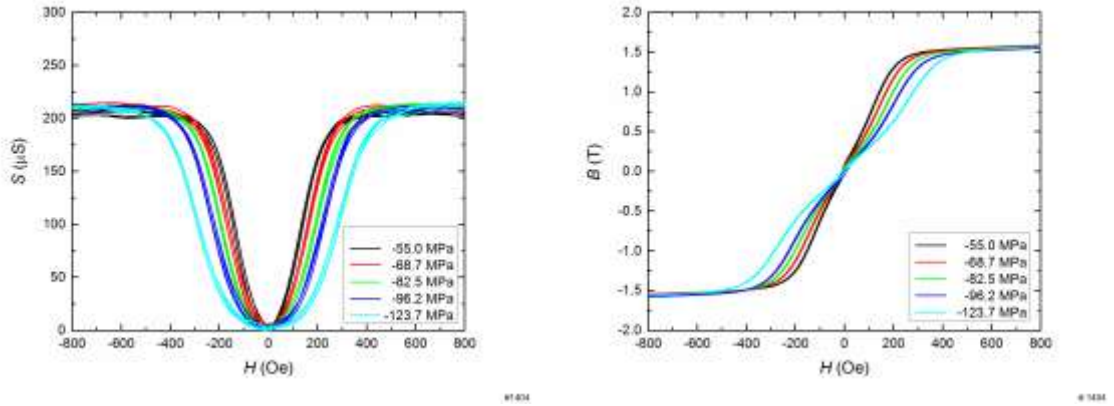

- Piezomagnetic constants d_{33} and relative permeability μ_{33} as a function of magnetic field *H* under compressive stresses of –55.0, –68.7, –82.5, –96.2, and –123.7 MPa.

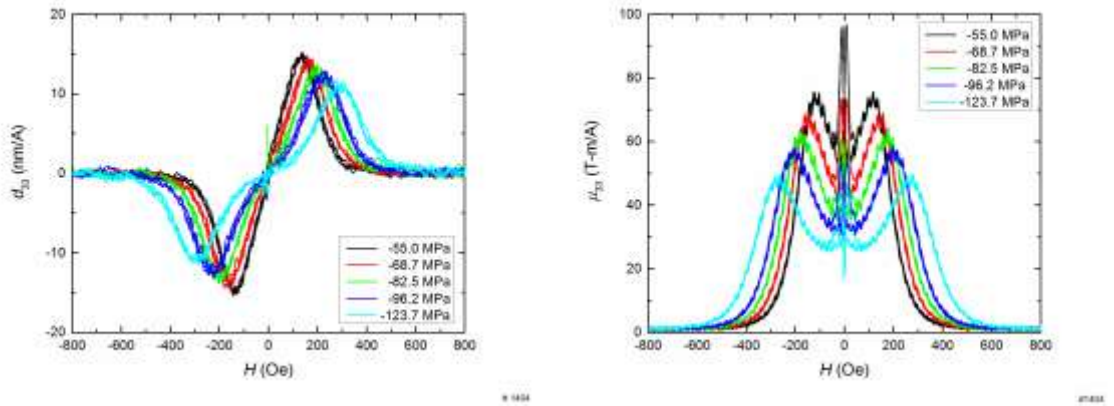

- Strain *S* and magnetization *B* as a function of stress *T* for magnetic fields of 150, 175, and 201 Oe.

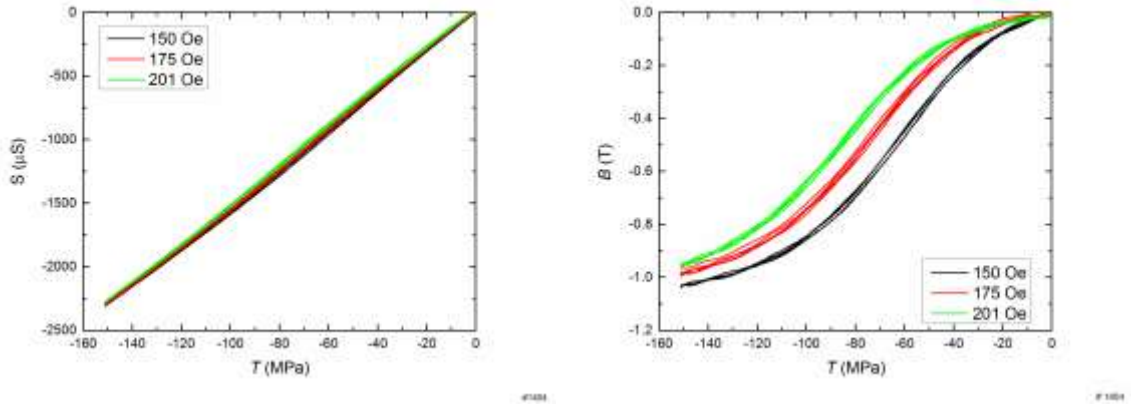

- Piezomagnetic constant d_{33}* and modulus E as a function of stress T for magnetic fields of 150, 175, and 201 Oe.

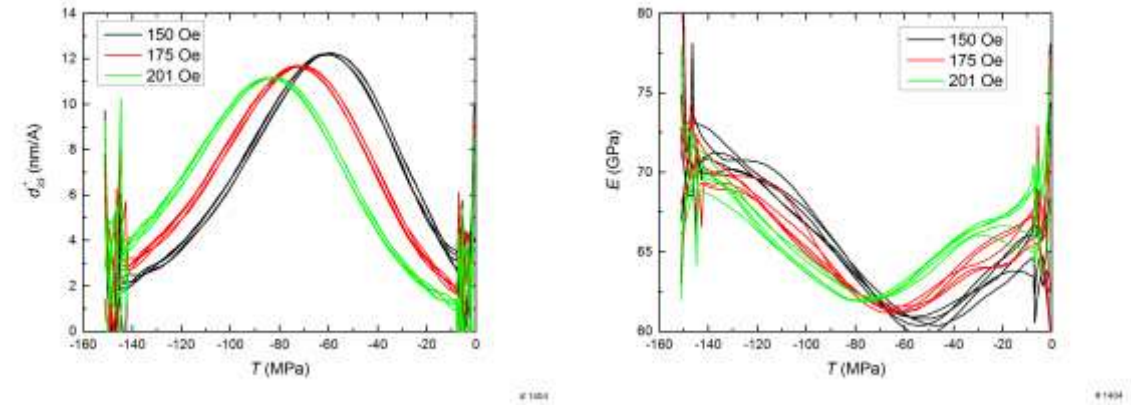

- Magnetostriction S and magnetization B as a function of magnetic field H under a constant stress of –55.2 MPa for repeated mountings in the experimental apparatus

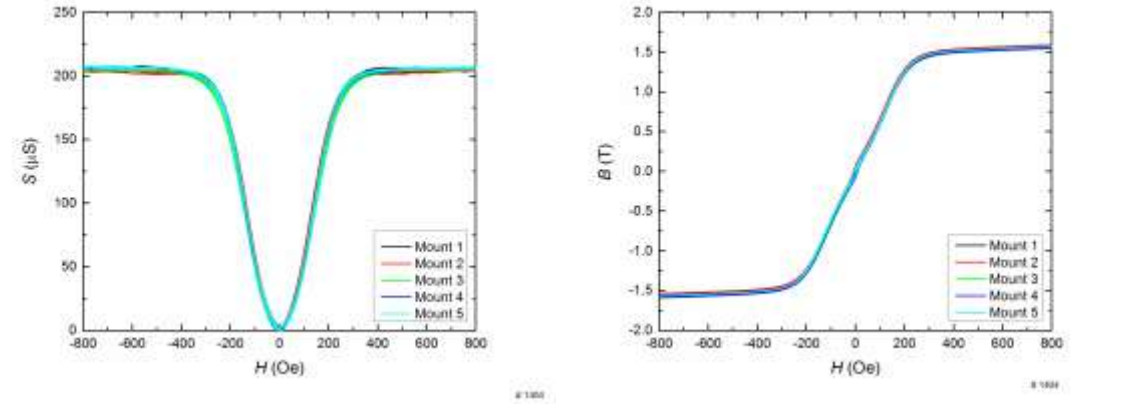

- Piezomagnetic constant d_{33} and relative permeability μ_{33} as a function of magnetic field H under a constant stress of –55.2 MPa for repeated mountings in the experimental apparatus

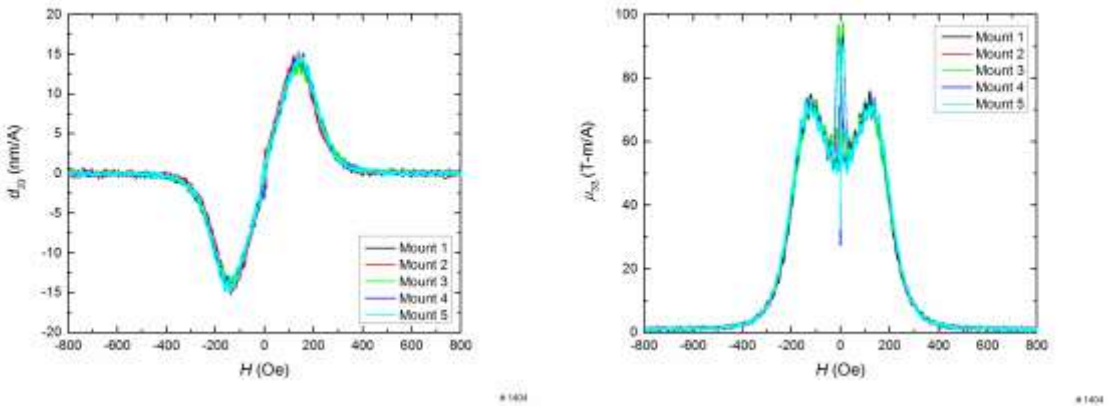

DISTRIBUTION

EXTERNAL

	Copies
DEFENSE TECHNICAL INFORMATION CENTER 727 JOHN J KINGMAN ROAD SUITE 0944 FORT BELVOIR, VA 22060-6218	2
ATTN: CODE 321 (MIKE WARDLAW) CODE 321 (JAN LINDBERG) OFFICE OF NAVAL RESEARCH BALLSTON CENTRE TOWER ONE 800 NORTH QUINCY STREET ARLINGTON VA 22217-5660	2 2
COMMANDER ATTN: CODE 213 (STEPHEN BUTLER) NAVAL UNDERSEA WARFARE CENTER 1176 HOWELL STREET NEWPORT RI 02841-1708	1
ATTN: ERIC SUMMERS JULIE SLAUGHTER ETREMA PRODUCTS INC 2500 N LOOP DRIVE AMES IA 50010	4 1

NSWCCD INTERNAL DISTRIBUTION

Code	Name	Copies
60		1
61	DeLoach	1
612	Roe	1
612	Jones	1
613	(Report Documentation Page)	1
614	(Report Documentation Page)	1
615	(Report Documentation Page)	1
616	(Report Documentation Page)	1
617	(Report Documentation Page)	1
617	(Report Documentation Page)	1
63	(Report Documentation Page)	1
65	(Report Documentation Page)	1
66	(Report Documentation Page)	1
3442	(TIC)	1
932	Verrinder	1


NAVSEA
WARFARE CENTERS
Carderock